THE JOURNAL OF COMPARATIVE NEUROLOGY 485:218–239 (2005)

Architecture and Neurocytology of Monkey Cingulate Gyrus

BRENT A. VOGT,[1,2]* LESLIE VOGT,[1,2] NURI B. FARBER,[3] AND GEORGE BUSH[4,5]
[1]Cingulum NeuroSciences Institute, Manlius, New York 13104
[2]State University of New York Upstate Medical University, Syracuse, New York 13210
[3]Department of Psychiatry, Washington University, St. Louis, Missouri 63110
[4]Department of Psychiatry, Harvard Medical School, Boston, Massachusetts 02115
[5]Massachusetts General Hospital, Charlestown, Massachusetts 02129

ABSTRACT

Human functional imaging and neurocytology have produced important revisions to the organization of the cingulate gyrus and demonstrate four structure/function regions: anterior, midcingulate (MCC), posterior (PCC), and retrosplenial. This study evaluates the brain of a rhesus and 11 cynomolgus monkeys with Nissl staining and immunohistochemistry for neuron-specific nuclear binding protein, intermediate neurofilament proteins, and parvalbumin. The MCC region was identified along with its two subdivisions (a24′ and p24′). The transition between areas 24 and 23 does not involve a simple increase in the number of neurons in layer IV but includes an increase in neuron density in layer Va of p24′, a dysgranular layer IV in area 23d, granular area 23, with a neuron-dense layer Va and area 31. Each area on the dorsal bank of the cingulate gyrus has an extension around the fundus of the cingulate sulcus (f 24c, f 24c′, f 24d, f 23c), whereas most cortex on the dorsal bank is composed of frontal motor areas. The PCC is composed of a dysgranular area 23d, area 23c in the caudal cingulate sulcus, a dorsal cingulate gyral area 23a/b, and a ventral area 23a/b. Finally, a dysgranular transition zone includes both area 23d and retrosplenial area 30. The distribution of areas was plotted onto flat maps to show the extent of each and their relationships to the vertical plane at the anterior commissure, corpus callosum, and cingulate sulcus. This major revision of the architectural organization of monkey cingulate cortex provides a new context for connection studies and for devising models of neuron diseases. J. Comp. Neurol. 485:218–239, 2005.

Indexing terms: cingulate cortex; neurofilament proteins; cingulate motor areas; midcingulate cortex; retrosplenial cortex; pyramidal neurons

The primate cingulate gyrus was early considered to be a uniform structure with a role in limbic function (Broca, 1878; Papez, 1937; MacLean, 1990). Although it has also been recognized to have a dual structure with different connections (Baleydier and Mauguiere, 1980; Vogt et al., 1987) and with an executive function in the anterior and evaluative role for the posterior parts (Vogt et al., 1992), many cytoarchitectural studies showed the human cingulate gyrus to be more complex than the dual model suggests (Smith, 1907; Brodmann, 1909; Vogt and Vogt, 1919; von Economo and Koskinas, 1925; Rose, 1927) and numerous human functional imaging studies show that cingulate cortex is involved in more than just two essential functions. Structure/function correlations with human neurocytology and imaging, electrical stimulation, and stroke findings suggest there are four rather than just two regions (Vogt et al., 1997, 2004). The four regions are perigenual anterior cingulate cortex (ACC), midcingulate cortex (MCC), posterior cingulate cortex (PCC), and retrosplenial cortex (RSC).

A key aspect of the four-region model is division of Brodmann's (1909) ACC into a perigenual and midcingulate regions and this differentiation is pivotal to under-

Grant sponsor: National Institutes of Health; Grant number: NINDS RO144222; Grant number: NIAAA AA06916 (to B.A.V.); Grant number: NIA PPG11355 (to N.B.F., B.A.V.); Grant sponsor: National Science Foundation; Grant number: 242229 (to G.B).

*Correspondence to: Brent A. Vogt, Cingulum NeuroSciences Institute, 4435 Stephanie Drive, Manlius, NY 13104. E-mail: bvogt@twcny.rr.com

Received 12 October 2004; Revised 13 December 2004; Accepted 13 December 2004

DOI 10.1002/cne.20512

Published online in Wiley InterScience (www.interscience.wiley.com).

standing the functional organization of primate cingulate cortex. The ACC has reciprocal connections with the amygdala, projections to the nucleus of the solitary tract and dorsal motor nucleus of the vagus, regulates autonomic output, and stores emotional memories (Neafsey et al., 1993; Vogt et al., 1997, 2003, 2004). In contrast, the MCC regulates skeletomotor function through its projections to the spinal cord, receives only modest amygdala input to its anterior part and does not directly regulate autonomic outputs, and has a prominent projection from posterior parietal cortex (Vogt et al., 1997, 2004). The posterior part of human MCC contains the primitive gigantopyramidal motor field of Braak (1976), which in monkey is termed area 24d or the caudal cingulate motor area (cCMA). The cCMA has somatotopically organized skeletomotor projections to the spinal cord (Biber et al., 1978; Dum and Strick, 1991, 1993, Matelli et al., 1991; Luppino et al., 1991) and large pyramids in layer V that express intermediate neurofilament proteins (Nimchinsky et al., 1996, 1997) and neurons that project to motor cortex (Morecraft and Van Hoesen, 1992; Nimchinsky et al., 1996). The rostral cingulate sulcus has the rostral cingulate motor area (rCMA), which differs from the cCMA because the former has longer premovement activity onset, responses associated with the changing reward features of a movement, and projections to the presupplementary motor part of the striatum rather than to that part which receives primary motor cortex input and differences in corticocortical connections (Shima et al., 1991; Luppino et al., 1991; Van Hoesen et al., 1993; Rizzolatti et al., 1996; Shima and Tanji, 1998; Takada et al., 2001; Akkal et al., 2002). Finally, the duality of the human MCC has been established with anterior (aMCC) and posterior (pMCC) parts based on the two CMAs and different cytoarchitectures (Vogt et al., 2003).

Progress over the past decade in human neuroscience has raised many questions about the organization of the primate cingulate gyrus, particularly in the monkey, and these questions frame the present research. First, Zilles et al. (1996) showed a caudal area cmc1 in human with very large neurons in layers III and V that appears to parallel Braak's primitive gigantopyramidal field, and they identified a rostral extension termed cmc2 with smaller, although still large, neurons. This latter area might regulate muscles in the hindlimb, lower trunk, and tail (Rizzolatti et al., 1996) and may have the highest density of cingulospinal projection neurons (Dum and Strick, 1991), whereas cmc1 may regulate forelimb, upper trunk, and neck muscles (Rizzolatti et al., 1996). The cmc dichotomy has not been considered in the monkey nor have transitions from cingulate to premotor areas in the cingulate sulcus dorsal bank.

Second, a previous map of monkey cingulate cortex shows a simple transition from agranular area 24 to granular area 23; presumably due to a buildup in layer IV neurons similar to that shown by Brodmann (Vogt et al., 1987; Morecraft et al., 2004). Recent human studies show a more complicated transition pattern, including differentiation of layer Va in midcingulate cortex (Vogt et al., 1995, 2003, 2004), which includes a neuron-dense layer Va in pMCC, a dysgranular division of area 23 (area 23d), and a dorsal posterior cingulate cortex (d23a/b) with granular layers IV and Va. This sequence of transitional events needs to be evaluated in the monkey. It is also unclear whether area 32 extends dorsal to the rostral CMA as it does in human. Thus, a complete analysis of MCC as a functional and cytological entity and its adjacent areas is needed in the monkey.

Third, the monkey PCC has been differentiated into two parts on the basis of thalamic (Shibata and Yukie, 2003), prefrontal (Vogt and Barbas, 1988), and superior temporal (Yukie, 1995) connections. These two divisions also have been immunohistochemically and functionally defined in human (Vogt et al., personal communication). It is not known to what extent the monkey PCC has dorsal (dPCC or area d23a/b) and ventral vPCC or area v23a/b) divisions. Where is the junction between areas p24a′/b′ and area 23a/b and between areas 24d and 23c in the caudal cingulate sulcus? Also, what are the characteristics of the border between pMCC and PCC, and is there a cytological basis for dorsal and ventral area 23a/b?

Fourth, from a methodological perspective, it should be noted that cytoarchitectural studies often use low magnification optics to assess Nissl preparations and often focus on only a part of the gyrus. Cellular resolution using neuron-specific nuclear binding protein (NeuN) has the benefit of not staining glial or vascular cells and enhances laminar differences not apparent with Nissl stains. Immunohistochemistry can be used to assess particular proteins expressed by specific neurons as with antibodies to intermediate nonphosphorylated neurofilament proteins (NFP; SMI32 antibody) for large pyramidal neurons and calcium-binding proteins for local-circuit interneurons. Dombrowski et al. (2001) evaluated different classes of calcium-binding protein-expressing neurons in monkey frontal lobe and concluded that parvalbumin was the most effective in specifying structural differences among areas. Parvalbumin-immunoreactive neurons are in all layers, they are an interneuron marker that complements the large neuron labeling of SMI32, and it is valuable for distinguishing areas on the cingulate gyral surface and dorsal bank (Nimchinsky et al., 1997). Because different laminar patterns of neuronal markers make some markers better to identify individual areas (Carmichael and

Abbreviations

ac	anterior commissure
ACC	anterior cingulate cortex
cas	callosal sulcus
ces	central sulcus
cgs	cingulate sulcus
cml	caudomedial lobule; mainly area v23b
rCMA, cCMA	cingulate motor areas, rostral or caudal
gcc	genu of the corpus callosum
ir	immunoreactivity
MCC	midcingulate cortex
mr	marginal ramus
NeuN, N	neuron-specific nuclear binding protein
NFP	neurofilament proteins
PCC	posterior cingulate cortex
Parv, P	parvalbumin
pc	posterior commissure
pos	parieto-occipital sulcus
rs	rostral sulcus
RSC	retrosplenial cortex
scc	splenium of the corpus callosum
SEM	standard error of the mean
SMI32, S	antibody to nonphosphorylated intermediate neurofilaments
spls	splenial sulcus
VCA	vertical plane at the anterior commissure

Price, 1994), we added parvalbumin to assess cingulate neurocytology.

The strategy for this work involved three stages. First, a re-analysis of an original Nissl-stained, rhesus monkey case was performed to assess the midcingulate concept in monkey with classic methods, and a re-analysis considers the border and transition between agranular area 24 and granular area 23. Second, immunohistochemistry for NeuN, NFP, and parvalbumin macrophotography was used to evaluate each of the above questions raised from the perspective of human cortex and high-magnification neurocytology analyzed to determine the features of each area. Third, cases were flat mapped with reference to the vertical plane at the anterior commissure (VCA) to coregister these and other findings to resolve questions of structure and function correlations.

MATERIALS AND METHODS

Subjects and tissue processing

One adult, male rhesus monkey was used to initiate these studies by serving as a point of re-analysis from Vogt et al. (1987). The case was embedded in celloidin, and the left hemisphere was cut coronally at a 30 μm thickness into 285 sections and stained with cresyl violet. Once a survey was completed and documented in this case, 11 adult cynomolgus monkeys were prepared. These animals (7 female, 4 male; weight, 4.02 ± 1.06 kg) were anesthetized with ketamine (15 mg/kg, i.m.) and then with sodium pentobarbital (40 mg/kg, i.v.) according to a protocol approved by the Committee for the Humane Use of Animals at SUNY Upstate Medical University (Syracuse, NY), Wake Forest University School of Medicine (Winston-Salem, NC), and Washington University (St. Louis, MO). The animals were perfused intracardially in the following sequence: (1) 1 ml of 0.1% sodium nitrite injected into the heart, (2) 300 ml 0.9% cold sodium chloride, (3) 1 liter of 1% cold paraformaldehyde, (4) 1.5 liters of 4% cold paraformaldehyde over a period of 40 minutes. Brains were removed, bisected, post-fixed in 4% paraformaldehyde for 2–3 days in the refrigerator, and put through a graded series of 10%, 20%, and 30% sucrose until the brain sunk in each solution for refrigerator storage and cutting.

These 11 animals were selected from a larger collection because they had full series through cingulate cortex with NeuN and SMI32 immunohistochemistry, and three had an additional series with parvalbumin. Each case was oriented perpendicular to the anterior–posterior commissural line (ac-pc plane; Figs. 1, 2) and digitally photographed. Three coronal blocks were cut, and the brains were rephotographed. All but one case was cut in the coronal plane in a cryostat at a 40 μm thickness into six series. One series each was prepared for NeuN (Chemicon, Temecula, CA), SMI32 (Sternberger Monoclonal, Baltimore, MD) for NFP followed by counterstaining with thionin, and parvalbumin (Chemicon) in the following manner. Sections were pretreated with 75% methanol/25% peroxidase, followed by a 3-minute pretreatment with formic acid (NeuN only) and then a washing with distilled water and two washes in phosphate buffered saline (PBS, pH 7.4). Sections were incubated in primary antibody in PBS (dilutions: SMI32, 1:10,000, mouse; NeuN, 1:1,000, mouse) and parvalbumin (1:3,000, mouse) containing 0.3% Triton X-100 and 0.5 mg/ml bovine serum albumin (BSA) overnight at 4°C. After the sections were incubated in the primary antibody, they were then rinsed in PBS and incubated in biotinylated secondary antibody at 1:200 in PBS/Triton-X/BSA for 1 hour. After rinses in PBS, sections were incubated in ABC solution (1:4; Vector Laboratories, Burlingame, CA) in PBS/Triton-X/BSA for 1 hour followed by PBS rinses and incubation in 0.05% diaminobenzidine, 0.01% H_2O_2 in a 1:10 dilution of PBS for 5 minutes. After final rinses in PBS, sections were mounted, air-dried, counterstained with thionin, dehydrated, and cover-slipped. Before a final series was prepared, two to three sections were processed from at least three blocks distributed over the cingulate gyrus according to optimal reaction conditions to check the reaction before a complete series was prepared to ensure that all reagents and tissues were optimal. Each new batch of antibody was tested for specificity by excluding the primary antibody from the reaction, including the peptide blocker parvalbumin in the reaction, and all sections were counterstained to ensure that nuclei/layers with high immunoreactivity were so stained. Once the sections were mounted, they were either dried and cover-slipped or first counterstained with thionin for 3 min (0.05% thionin, 3.7% sodium acetate, 3.5% glacial acetic acid, pH 4.5). This counterstaining of SMI32 ensured accurate localization of impregnated neurons to particular layers in instances where only a few layers of neurons were immunoreactive.

Analytical methods

The range of body weights for eight cynomolgus monkeys was 3–4.3 kg, and there was one outlier (i.e., 2 SD from mean) of 6.8 kg. Because variation in brain sizes should determine the number and value of flat maps needed for this analysis, calibrated digital photographs of the medial surface were used to calculate the distance between the rostral tip of the genu and caudal tip of the splenium of the corpora callosi. The range was 2.23–2.85 cm, and the mean ± SEM was 2.55 ± 0.217 cm. The largest animal in body weight had a distance of 2.8 cm, and there were two other animals with measurements of 2.8 and 2.85 cm. The correlation coefficient (r) of body weight and corpus callosum length for the 11 cases was 0.06, showing no correlation. Thus, flat map variation is dominated by measurement variation and the quality of staining and border localization rather than differences in the size of the cingulate gyrus.

Digital photographs of the medial surface were oriented parallel to the ac-pc line, and a perpendicular plane was defined at the anterior commissure (VCA). The medial surface was flattened in one dimension only so that measurements from the vertical plane at the anterior commissure would be accurate in the rostrocaudal or "y" axis. Maps were generated according to the following procedure: (1) The digital image of the medial surface was rotated so the long axis of the corpus callosum was horizontal. (2) The superior frontal and parietal sulci were removed and coronal cutting surface orientations marked. (3) The dorsal edge of the corpus callosum was drawn and repositioned above the photograph. (4) Matched sections of NeuN, SMI32, and parvalbumin were selected at equal distances for 19 levels, and each was digitally photographed at 1× including a 1-mm calibration bar and printed as triads. Each triad of photographs was printed together on a single page. (5) Measurements were made at mid-cortical levels of the distance between each gyral apex

and sulcal fundus, and dots were plotted as the distance from the dorsal surface of the corpus callosum on the flat map. In two instances, the flat map was coregistered to surface renderings in other studies using different layers in Photoshop. The coregistration was performed by aligning the dorsal edge of the corpus callosum, anterior commissure, cingulate sulcus, and paracentral lobule in the flat map with those in each data set from Dum and Strick (1991) and Rizzolatti et al. (1996).

Once a survey series of low-magnification prints was available, a centroid level was defined for each area (i.e., approximate center in all planes of section) using the flat map and higher magnification assessments and documentation were made and the digital images were imported into different palette layers in Adobe Photoshop 6.0. This strategy was crucial, because the three immunohistochemical sections from the each area were temporarily merged to ensure exact alignment of all cortical layers. This was accomplished by reducing the opacity of an overlying layer (SMI32 or parvalbumin) and coregistering the sections based on pia matter, white matter, and large neurons in layers Va and IIIc (Figs. 9, 12).

RESULTS

Rhesus monkey

The gyral surface of a Nissl-stained rhesus monkey case was evaluated to determine whether the characteristics of transition from area 24 to area 23 observed in human studies are applicable to the monkey. Of the 240 sections through the left cingulate gyrus, 30 were photographed at the "b" subdivisions to assess cytoarchitectural transition along the full length of the gyrus. An equally spaced sample series of 10 sections are shown in Figure 1 where magnifications were selected to emphasize mid-cortical layers, where the transition from agranular to granular cortex occurs, to identify the location of the first layer IV neurons. The star at section 159 in Figure 1 refers to the original border between areas 24 and 23 (Vogt et al., 1987), and this border is 3 mm caudal to the VCA. The first evidence of a layer IV is in section 191 (arrow to layer IVd). At this level, there is a bridge of neurons between layers IIIc and Va, and this lack of a complete layer IV is characteristic of a dysgranular layer IV. Because the photographs are aligned at the superficial border of layer Va, it can be seen in section 159 that layer Va has a neuron-dense and granular appearance. This feature is characteristic of pMCC and may have contributed over the past century to mislocalization of the border between areas 24 and 23 when viewed with Nissl stains. No such neuron density occurs in layer Va of areas 24b or a24b′. In addition, claims that area 24 is dysgranular seem to be incorrect as can be seen in the high-magnification photographs of Figure 1; layer IIIc and Va directly abut in areas p24b′, a24b′, and 24b and there is no dysgranular layer.

Thus, the monkey has an MCC with areas a24′ and p24′ as in human, and there is a complex transition between areas 24 and 23, i.e., there is not a simple and progressive increase in the number of layer IV neurons. Rather, there is an increase in small-neuron density of layer Va of p24′ when compared with a24′, a dysgranular layer IV in area 23d, and a granular layer IV in area 23 in conjunction with a dense layer Va.

Cynomolgus monkey: Surface features and flat map

The medial surface is oriented parallel to the ac-pc plane in Figure 2 and the VCA drawn perpendicular thereto. The plane of coronal sections for this case is shown with arrowheads at the face of each of the three blocks. The corpus callosum was drawn at its dorsal border, placed above the medial surface photograph, and flattening produced in one dimension by extension from the corpus callosum. The retrosplenial areas were drawn by extension below the dorsal part of the corpus callosum. The splenial sulcus (spls) in this case is not directly attached to the cingulate sulcus (cgs), although there is a vascular indentation, and RSC (shaded area in Fig. 2) is placed ventral to the dorsal border of the callosum so that the overlying area 23 can be represented. The knee of the cgs at the inflection of the mr is noted with an arrow in Figure 1, because this is an important point of area confluence; just ventral to the knee area 23d on the gyral surface and area 23c in the cgs disappear. Finally, the caudomedial lobule forms the terminal part of the posterior cingulate gyrus and lies just dorsal to the ac-pc line.

Flat maps were generated like that shown in Figure 2 with reference to the genu of the corpus callosum, VCA, knee of the cgs, and caudal edge of the splenium of the corpus callosum. To verify that the brains were a similar size, the corpora callosi were measured from the rostral tip of the genu to the caudal tip of the splenium. This distance was 2.55 ± 0.217 cm, and there was no correlation between body weight and the length of the corpus callosum. Thus, coordinates in the "y" and "z" planes for any area in this case are similar for all adult cynomolgus monkeys with less than a 10% measurement error.

Although the basic layout of cynomolgus cingulate cortex is similar to that reported for rhesus monkey, there have been several modifications based on rhesus monkey (Vogt, 1993; Vogt et al., 1997) and human observations (Vogt et al., 2003, 2004) and these studies are reported herein. First, MCC is identified with a prime following area 24 to refer to its posterior placement and agranular form, and it is composed of seven unique cytoarchitectures and three fundal extensions. Second, transition to the posterior cingulate region occurs by means of a dysgranular area 23d between areas 23 and p24′. Third, PCC is composed of dorsal and ventral divisions.

Anterior cingulate cortex

The ACC includes areas 32 and 24a rostral to the genu, area 24b dorsal to and 25 ventral to the genu, and area 24c with its fundal extension (f 24c) in the cgs. Figure 3 shows the most rostral part of ACC, including areas 24 and 32; ventral area 9 (9v) is described below, because it is more fully elaborated dorsal to the genu. Area 32 is a dysgranular cortex with a thin layer IV. Only layer Va neurons express NFPs, with very few such cells in layers IIIc and Vb (Fig. 3). In contrast, area 24c has a broad layer of NFP-expressing neurons in layer V, but activity in layer IIIc is still weak. Generally, the large neurons in both divisions of layer V are larger in area 24c than in area 32 (Fig. 3, NeuN at high magnification). Layer VI in area 24c is also much more dense and differentiated than it is in area 32.

Subgenual cingulate cortex is composed of areas 24a, 25, and a frontal cortex extension termed area 10m (Car-

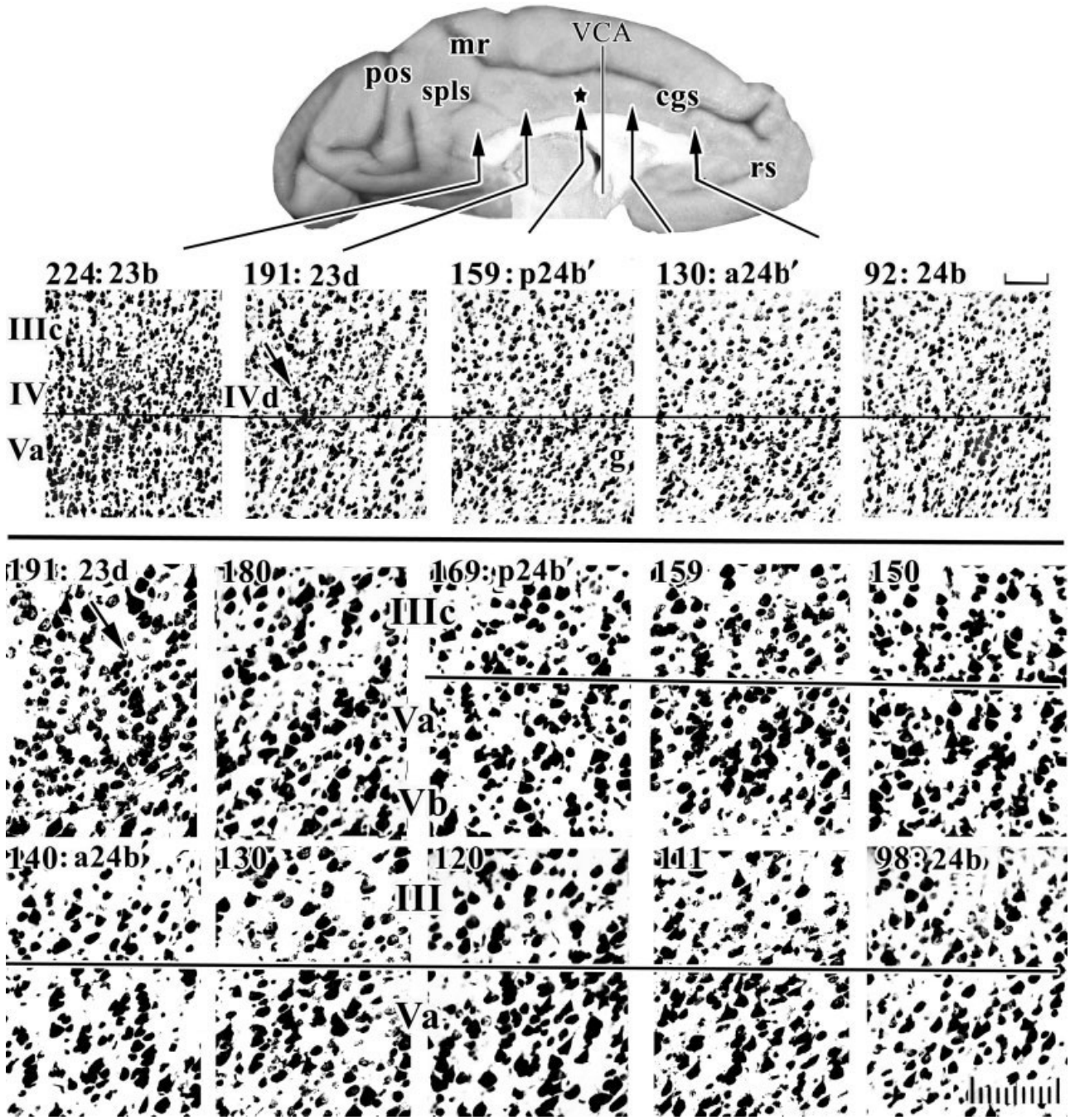

Fig. 1. Systematic sampling of cresyl violet-stained sections through a rhesus monkey case at two magnifications to assess architecture in "b" areas along the cingulate gyrus. Layers in sections for this and subsequent figures are aligned on the border between layers IIIc and Va or layers IV and Va. The star on the surface photograph is the position of the Brodmann border, and this "border" is 3 mm caudal to the vertical plane at the anterior commissure (VCA). The middle cortical layers are magnified to identify changes in small neuron densities in layers IV and Va. The first evidence of a layer IV is the dysgranular layer in area 23d (arrow, 191) and the dysgranular nature of this cortex is emphasized by the fact that layer IIIc/Va pyramids interact at one point, whereas area 23b caudally has an unbroken layer IV. Higher magnification shows that layer Va neurons in sections 98–130 are relatively large; in 140–159, large pyramids are somewhat smaller; whereas in 169–180, there are many small neurons in layer Va giving the appearance of a granular layer; this is not layer IV, however. cgs, cingulate sulcus; mr, marginal ramus; pos, parieto-occipital sulcus; rs, rostral sulcus; spls, splenial sulci. Scale bars = 100 μm.

michael and Price, 1994) as shown in Figure 4. Area 24a surrounds the genu and has a broad and undifferentiated layer V with substantial expression of NFPs. It also has a dense layer VI (NeuN) with many parvalbumin-immunoreactive (-ir) neurons and dendrites. In contrast, area 25 has much weaker NFP expression in layer V,

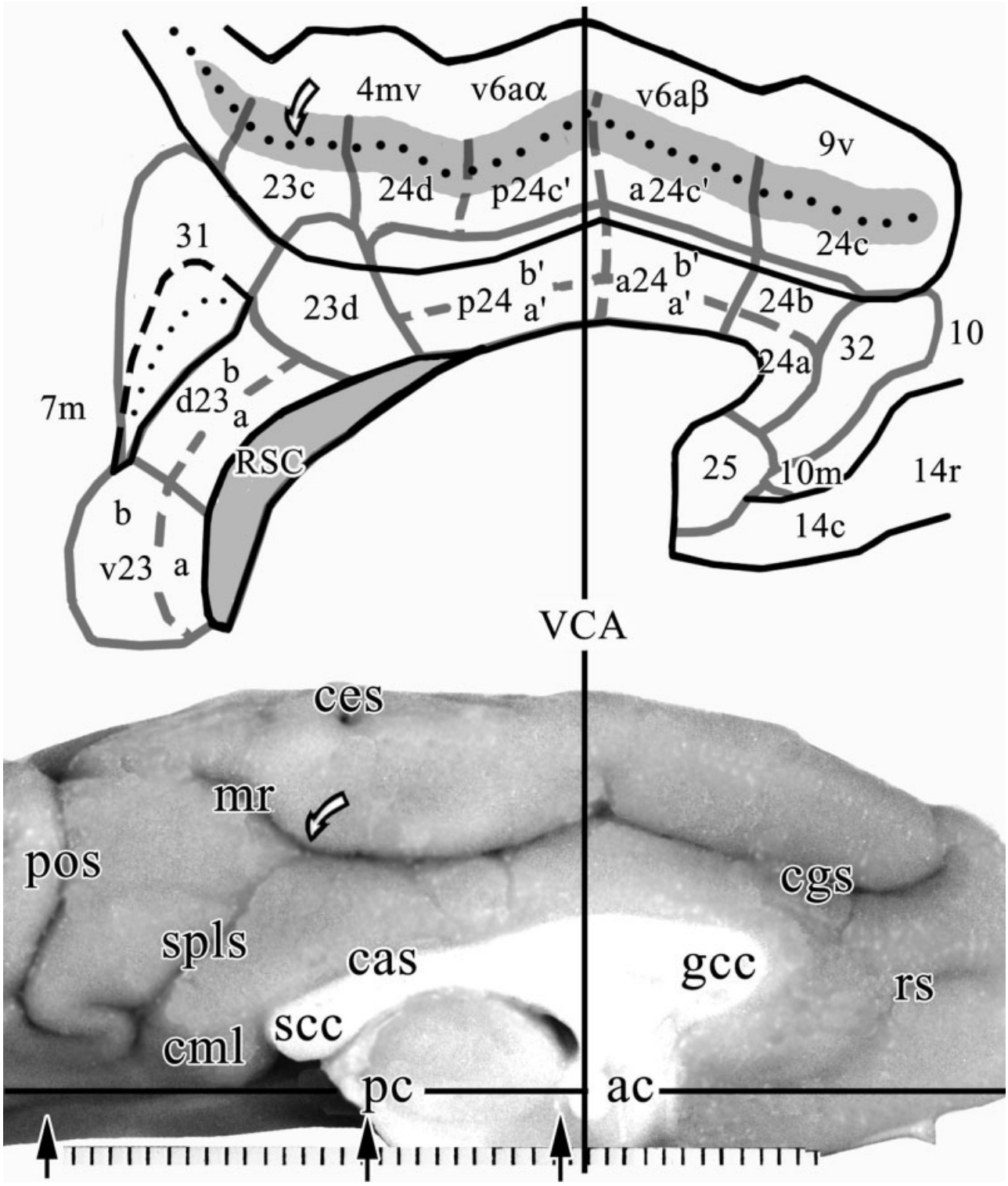

Fig. 2. Flattened reconstruction of the medial surface. The curved arrows designate the knee of the cingulate sulcus (cgs) where it emits the marginal ramus (mr). Flattening was performed in one dimension parallel to the VCA, and measurements from the VCA ("y" plane) reflect an accurate position, whereas measurements in the "z" and "x" planes are distorted. The fundal areas in the cgs are marked with shading as is the RSC in the callosal sulcus (cas). Outlines of the surface references are in black lines; each cytoarchitectural area is outlined with a thick and less opaque line; and the lines are dashed where subdivisions within an area are represented. Each division in the scale is 1 mm here and in subsequent medial surface photographs. For other abbreviations, see list.

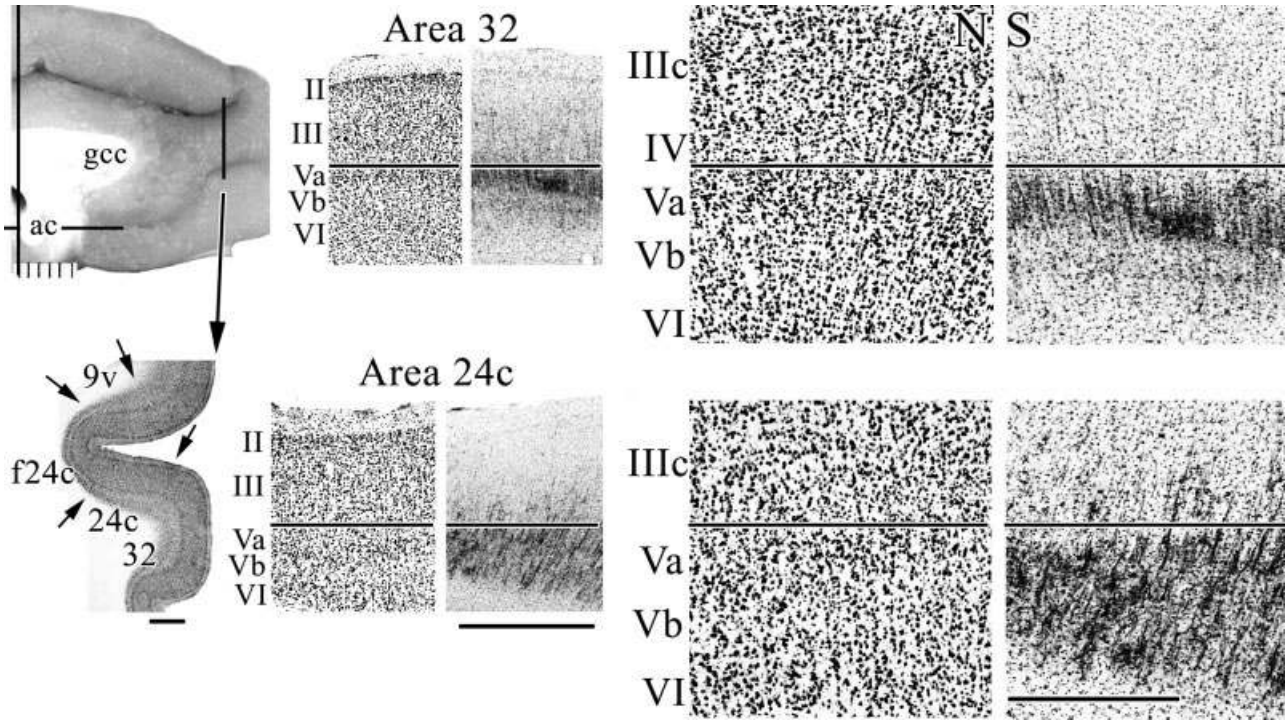

Fig. 3. Location and composition of areas 32 and 24c in the rostral cgs. Higher magnification shows the dysgranular layer IV in area 32 with NeuN (N), the lack of one in area 24c, and the much higher level of SMI32 immunoreactivity (S) in area 24c than area 32. For abbreviations, see list. Scale bars = 1 mm in left column and middle column; 500 μm in right column.

poorly differentiated layers V and VI, and fewer parvalbumin-expressing neurons in layer VI. Finally, area 10m has a dense layer V, relatively few NFP- and parvalbumin-expressing neurons and axonal plexuses, and a dysgranular layer IV. Although there are some parvalbumin-ir neurons in layer IV, no appreciable expression of NFPs occurs.

Cortex in sulcal ACC is shown in Figure 5. Pivotal to identifying individual layers in each cingulate area is using designations that are consistent with those for neocortex. Because cortical layers are differentially distorted in the fundus with deep layers being proportionately more stretched and superficial layers compressed, a level adjacent to area 4 was selected so that Betz neurons in layer Vb could be identified in SMI32 of a medioventral division of area 4 (4mv; Fig. 5). The Betz neuron closest to fundal area 24d (f24d) is circled, and the layers are identified in the fundus and on the ventral bank of the cgs in area 24d. The most-dense plexus and somatic impregnation is in layer Vb, whereas the neurofilament-sparse layer is in layer Va.

Area 24c has the thickest and least-differentiated NFP-expressing deep pyramidal layers V and VI of any part of the cingulate gyrus. There are also very few layer IIIc neurons expressing NFPs, whereas f24c does have an enhancement of them in layer IIIc. Layer Va is present (Fig. 5; NeuN); however, it overlaps to some extent with the NFP plexus, and the differentiation between layers Va and Vb is not pronounced. Parvalbumin expression shows two prominent layers of neuron labeling: one in layer Va and another in layer VI; the latter of which is more dense.

Cortex on the dorsal bank of the cgs is not "cingulate" in structure, although it has transitional features. The ventral area 9 is labeled 9v in Figure 5, and it has a slender layer Va, although it is less prominent than in area 24c. At higher magnification, the larger layer Va neurons are apparent in area 9v. The cingulate "signature" of a very neuron-dense layer Va that is disproportionate in relation to the less neuron-dense layer IIIc is not prominent in area 9v. Importantly, area 9v has very large layer IIIc pyramids (Fig. 5, NeuN and SMI32; high-magnification photographs), which is not true for area 24c. Parvalbumin also distinguishes between these areas, because the layer VI expression in area 24c is very weak in area 9v, whereas the number of labeled neuron and axons in superficial layers is much greater than in area 24c. Thus, although area 9v has transitional features characteristic for both areas 24c and 9, it appears to share more features with area 9, in particular, the fully developed and NFP+ layer IIIc pyramidal neurons and very large pyramids in both divisions of layer V.

Cortex on the dorsal and ventral banks of the cingulate sulcus

Most of the cingulate gyrus abuts frontal cortex, except for part of the PCC. In addition to defining the specific organization of each cingulate area, an important question is to what extent cortex on the dorsal bank of the sulcus is "cingulate" or "frontal" as partially considered above. This question is best resolved with low-magnification macrophotographs of the entire sulcus as in

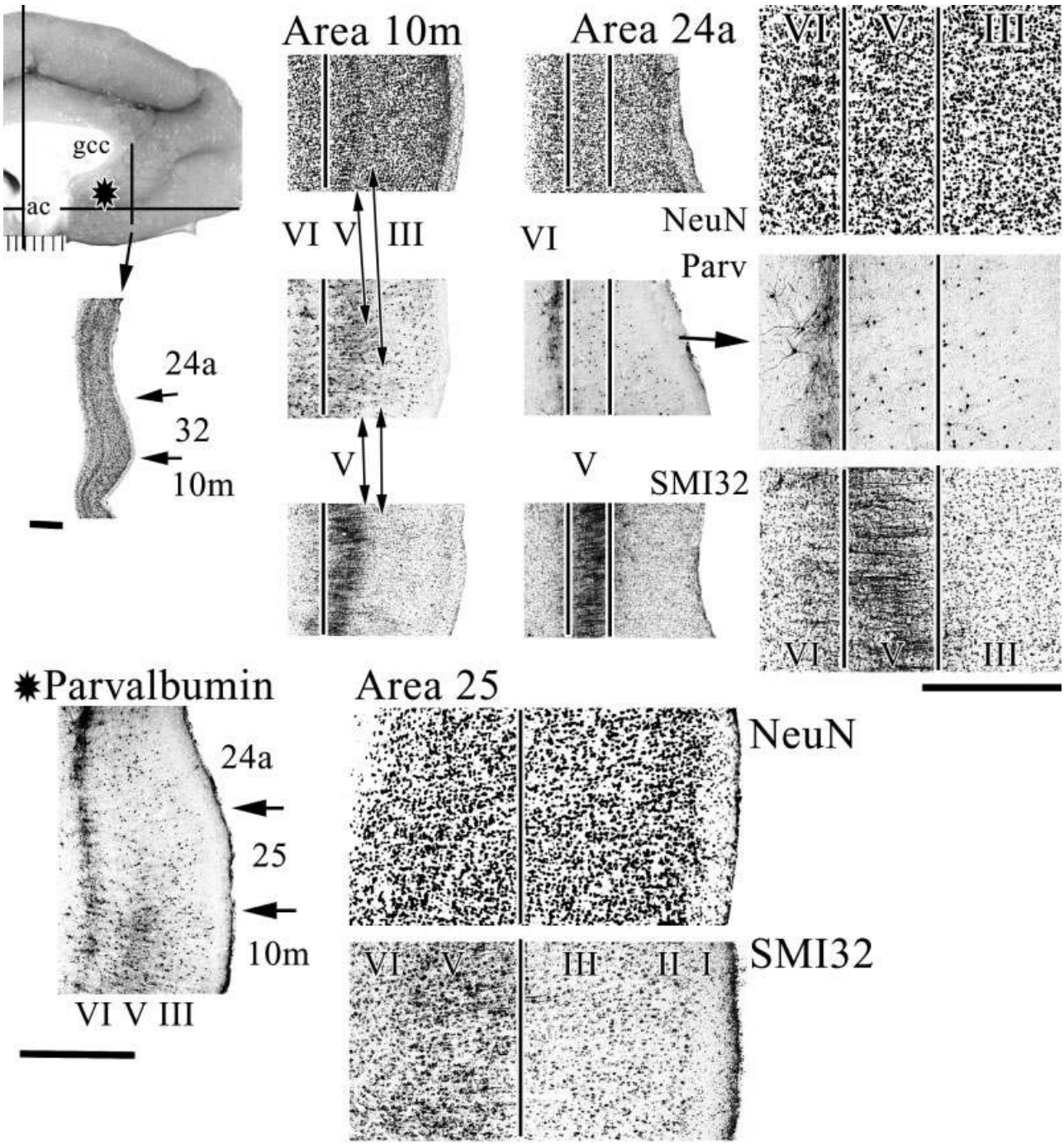

Fig. 4. The ventral and rostral areas are differentiated with NeuN, SMI32, and parvalbumin (Parv). A Parv plexus is particularly notable in layer VI of area 24a and differentiation of areas 25 and 10m is clear in all preparations. The composition of area 24a is shown at higher magnification (arrow in Parv), with the homogeneous layers III, V, and VI (NeuN) and heavy NFP expression in layer V, and a similar motif is observed in area 25 (SMI32), although NFP expression is much more limited in this latter area. For abbreviations, see list. Scale bars = 1 mm in left (top, bottom); 0.5 mm in right.

Figure 6 and higher magnifications to detail particular neuron structures and protein expression patterns. Figure 6 shows three rostrocaudal levels of the cingulate sulcus and shows that the dorsal bank is quite different in architecture than the ventral bank. The fundal part of area a24c′ (fa24c′) abuts a ventral part of area 6aβ (v6aβ), the fundal division of area p24c′ (fp24c′) abuts the ventral division of area 6aα (v6aα), whereas a medioventral division of area 4 (4mv) abuts area 24d. Area 4mv is selected in Figure 6 to demonstrate how significantly different the

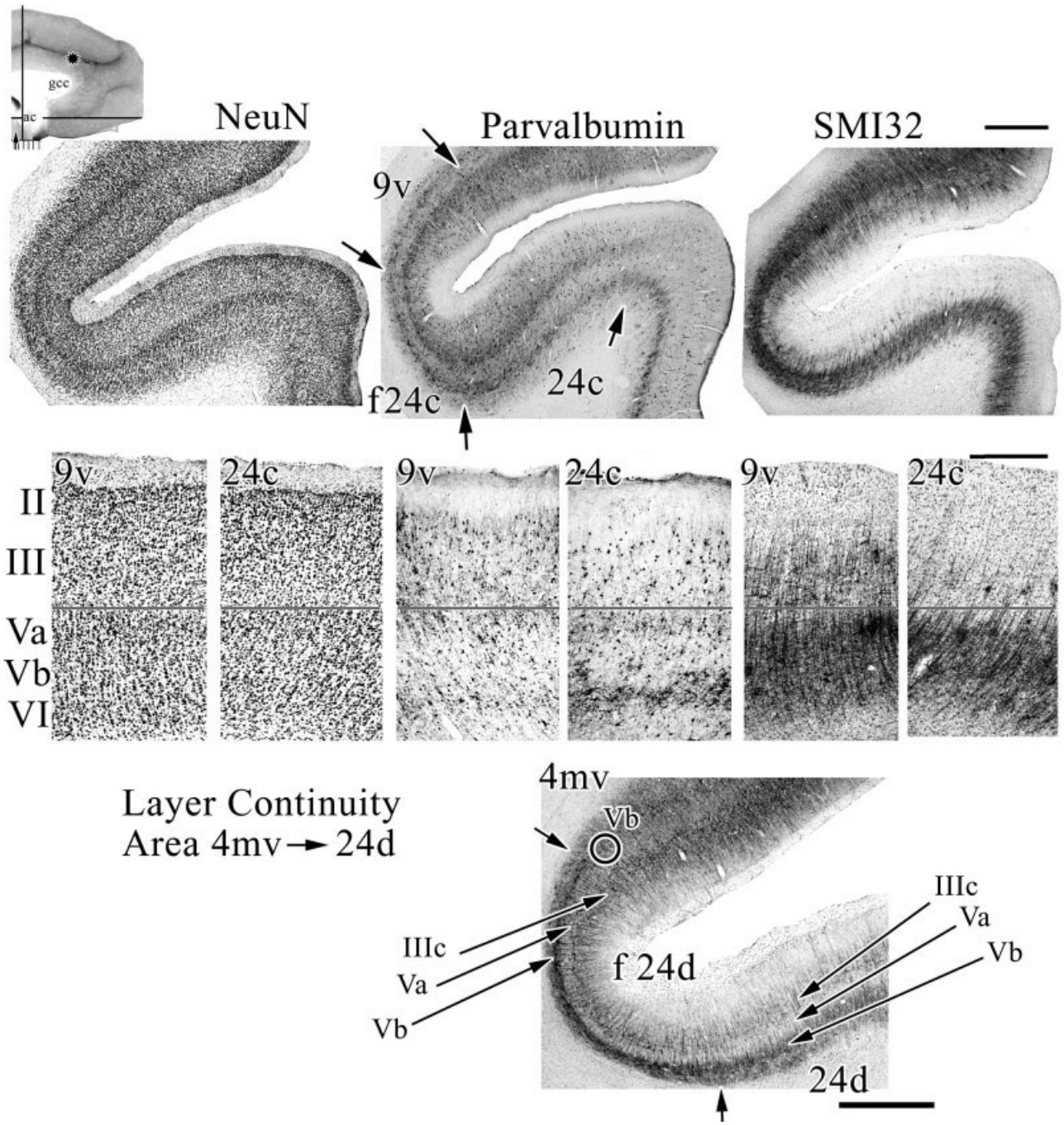

Fig. 5. Anterior cingulate sulcal cortex is composed of area 24c, its fundal extension (f24c), and area 9 in the dorsal bank. Although there is a bilaminar pattern in parvalbumin expression in areas 9v, f24c, and 24c, the level of staining in layer VI is much lower in 9v than area 24c, and the density of NFPs in layers IIIc and V is massive in comparison to that in area 24c. To ensure accurate designation of each layer around the fundus of the sulcus where cortical distortion is greatest, an SMI32 section was used from a posterior level where area 4mv abuts area 24d. The large Betz neurons in layer Vb are readily identified (one is circled), and this finding provides the gold standard for subsequent labeling of layers. The three neuron markers and merging the images for them ensures accurate laminar designations. For abbreviations, see list. Scale bars = 1 mm in top row and bottom row; 0.5 mm in middle row.

dorsal and ventral banks are at a higher magnification, although the low magnification at all levels is also quite compelling. Area 4mv is also useful in determining the location of layer Vb in SMI32 preparations (Fig. 5). Some differences between areas 4mv and 24d include the former's extensive numbers of NFP-expressing neurons in layer III and much larger Betz neurons in layer Vb (arrows in Fig. 6). Differences in superficial layer SMI32 immunoreactivity are obvious at all levels of magnification. Area 24d has a very dense layer Va with both large

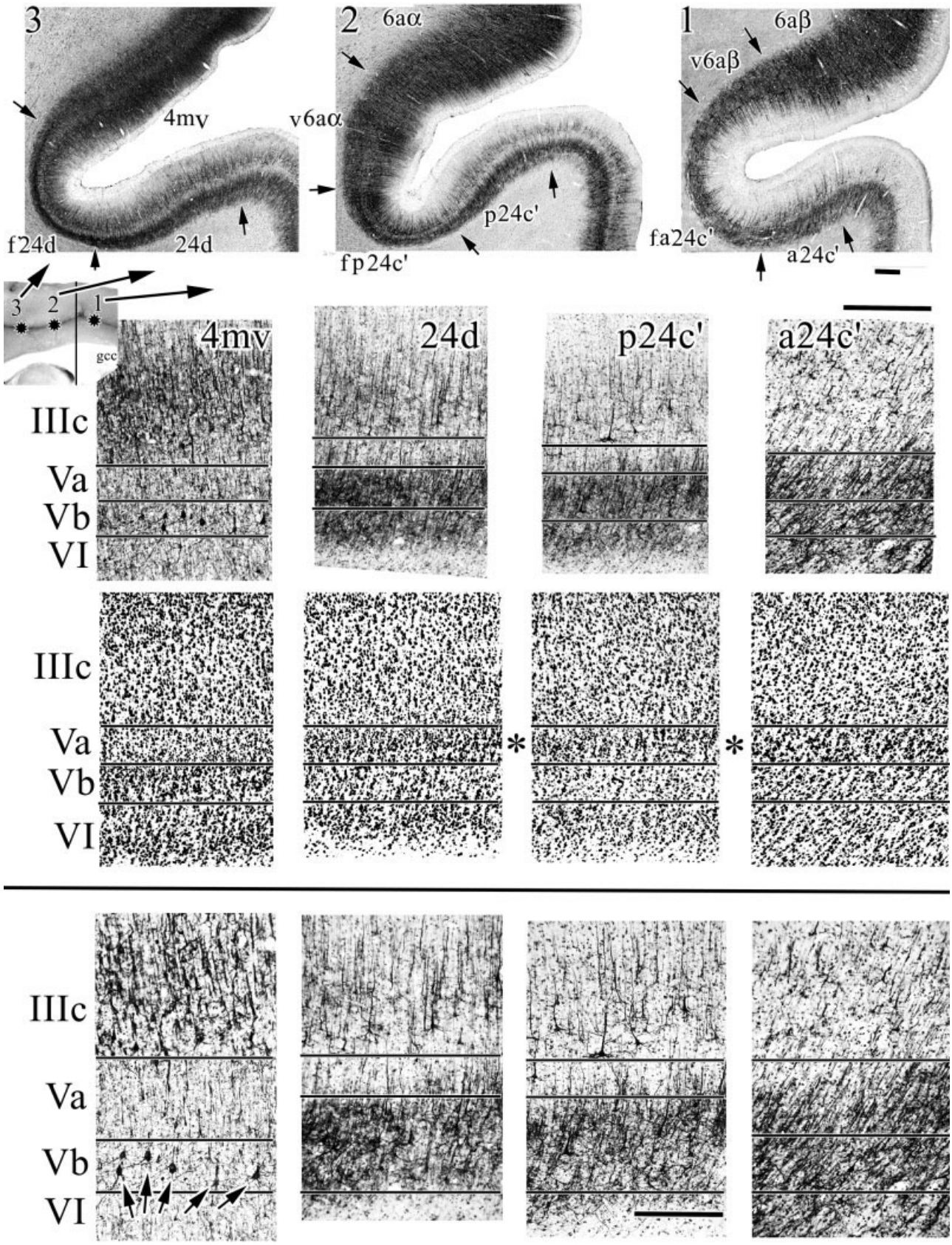

Fig. 6. Architecture of three levels of midcingulate cortex, including the dorsal bank of the cingulate sulcus. SMI32 shows that dorsal bank cortex does not share important similarities with cingulate cortex; the most profound differences being the very large Betz neurons in layers Vb of area 4mv (arrows in bottom left plate) and high density of NFP+ plexi throughout layer V in all cingulate areas. It also appears that fundal extensions have generally larger neurons in layers IIIc and Va. Even at intermediate levels of magnification, it can be seen that layer Va neurons are large and there is a progressive build-up in small neurons caudally in the sulcus (asterisks). gcc, genu of the corpus callosum. Scale bars = 0.5 mm (top); 0.5 mm (middle); 250 μm (bottom).

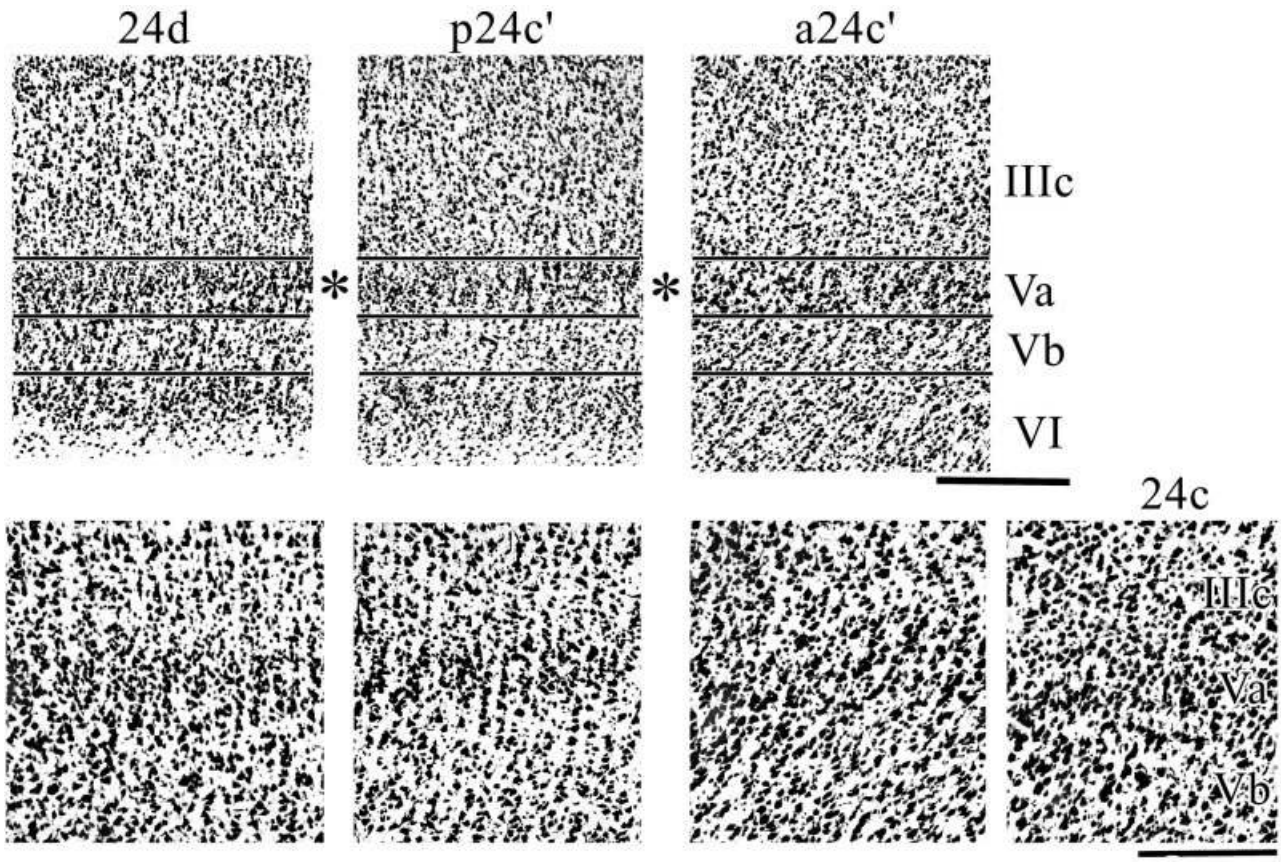

Fig. 7. High magnifications of NeuN in cingulate sulcal areas to assess the composition of layer Va. The asterisks are positioned the same way as in Figure 6. Neurons in this layer tend to be larger rostrally. At caudal levels, the neurons can be somewhat smaller and intermingled with many small neurons giving the layer a granular appearance. For abbreviations, see list. Scale bars = 500 μm (top row); 250 μm (bottom row).

and small neurons, as is characteristic of most cingulate areas, and this finding is not true of area 4mv.

Figure 1 shows a progressive, rostral-to-caudal build-up of small neurons in layer Va on the gyral surface of the rhesus monkey case and a similar trend occurs on the dorsal bank of the cingulate gyrus in the cynomolgus monkey. Figure 6 shows that neurons in layer Va of area a24c′ are larger and less dense than in area p24c′. Area 24d has a very neuron-dense layer Va with many small neurons intermingled with the larger ones (Fig. 7). Photographs at the asterisks were enlarged and rephotographed for Figure 7 to show the size and density of neurons in all sulcal areas, including area 24c. It appears that the overall largest neurons are in layer Va of area a24c′ when viewing NeuN preparations. Although this is also true for Nissl-stained tissue, NFP expression by the largest cingulate neurons shows that these latter are an infrequent part of cingulate architecture and are largest in the fundus adjacent to area 24d.

Cingulate sulcus fundal divisions

Curvature of cingulate cortex around the fundus of the cgs greatly attenuates architecture in this region. To the extent that these areas participate in skeletomotor regulation, these particular architectures can be considered the primary substrate for motor control as they are "stripped" of all but the largest neurons. The dorsal midcingulate gyral areas and their fundal extensions are shown in Figure 8. In all instances, the largest neurons labeled with SMI32 are larger in the fundal extension. It appears that the largest neurons on the cingulate gyrus are in layer Vb of areas fp24c′ and 24d. Of interest, the interneurons labeled with parvalbumin are also largest in layer Va of these same areas. These size differences are not as noticeable when viewing the total population of neurons with NeuN. Finally, the proportionate size differences also hold for layer IIIc neurons, which are relatively larger in fundal areas. Thus, the fundal cytoarchitectures are not simply the product of laminar and neuronal stretching, they are also a consequence of pyramidal neuron enlargement, and this may be necessary for these distorted areas to maintain their functional contribution to skeletomotor function.

Differentiation of cingulate gyral surface

As a general rule, the ventral "a" divisions are relatively homogeneous when compared with their dorsal "b" counterparts. Because this homogeneity in the former is due to a less well-differentiated layer Va, the "b" divisions also have a thicker and more-dense layer Va and many more

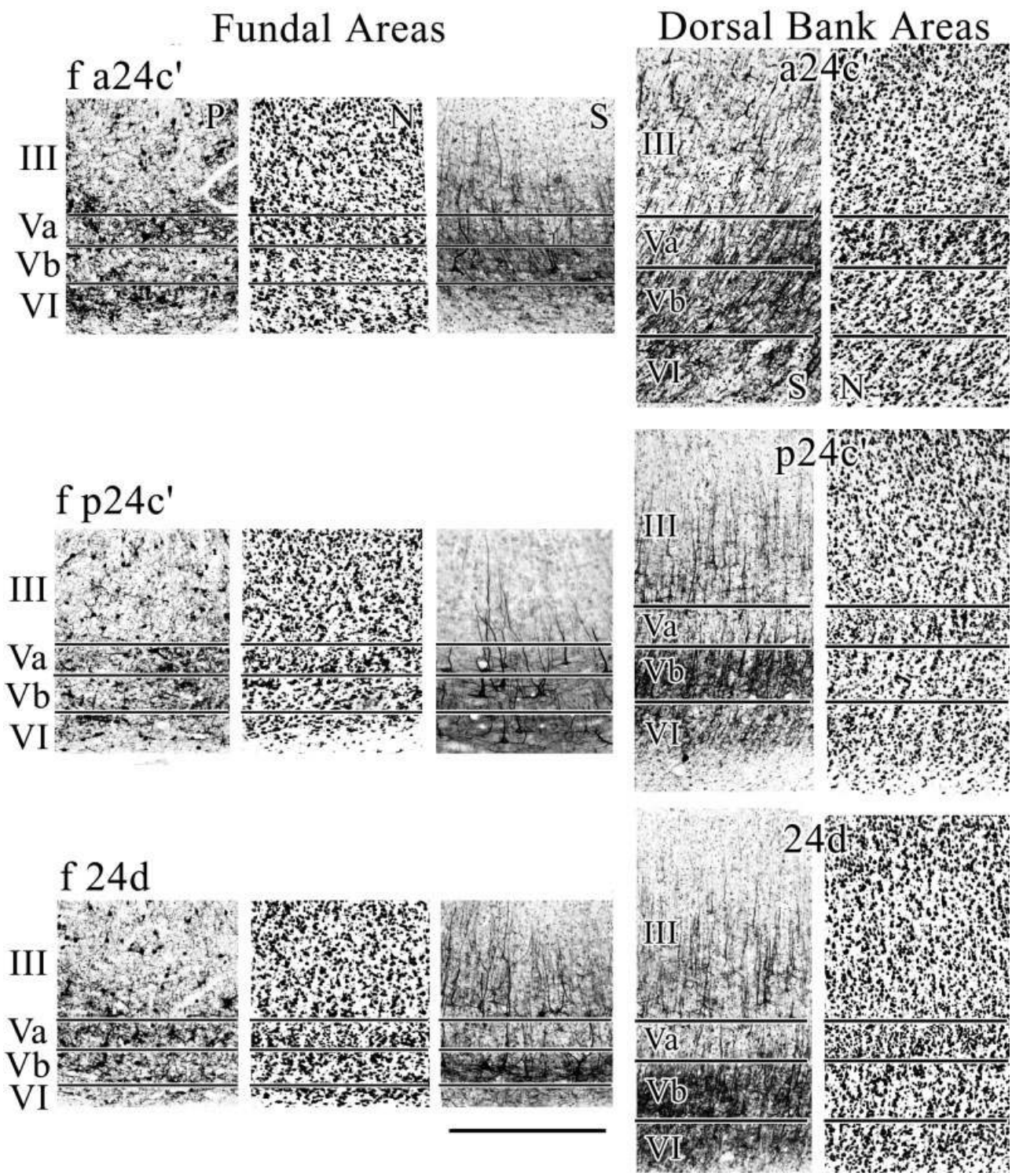

Fig. 8. The fundal extension of each cingulate gyrus area contains neurons that are generally larger both in SMI32, which emphasizes large, pyramidal-projection neurons, and in parvalbumin, which labels interneurons. "S" is SMI32 and "N" is NeuN. It appears the largest neurons are in layer Vb of area f p24c′. For abbreviations, see list. Scale bar = 500 μm.

NFP-expressing neurons in this layer than is the case for the "a" divisions. Figure 9 provides an intermediate level of magnification of "a:b" pairs of areas at all levels of the cingulate gyrus. The increase in layer Va neuron density and SMI32 immunoreactivity is present at the transition from area 24a to 24b and a24a′ to a24b′. This difference is not as pronounced in posterior cortex; however, differences in layer IIIc become more pronounced at caudal levels (i.e., areas d23a and d23b).

Level 4 in Figure 9 shows there is no a/b distinction at the dysgranular area 23d transition. A segment of this photograph was magnified 2× to show the dysgranular cortex with an intermingling of large pyramidal neurons in layers IIIc and Va. Also notice that SMI32-ir neurons are quite similar in all layers along the entire section photographed. Although the densities of NFP-expressing neurons in layer Va of both divisions of area d23 are similar, those in layer IIIc are much higher in the "b" than the "a" division of this area. Another important feature of cingulate architecture is discernible in Figure 9, where area 23 is not uniform in its dorsal and ventral parts. Area v23b has many more NFP-ir neurons in layers IIIc and Va, and they are substantially larger than is the case for area d23b as discussed in more detail in the next section.

Parvalbumin is a sensitive marker of each anterior and midcingulate area as shown in Figure 10. The following observations are notable: (1) Homogeneity of architecture in the dorsal part of area 24a is reflected in parvalbumin immunoreactivity; layer VI has a prominent plexus with diffuse labeling in layer III of area 24b; and these plexi are very prominent, particularly in layer Va in area 24c. (2) Midcingulate areas a24′ and p24′ have very high layer Va activity, but that in p24′ is more diffuse. (3) Parvalbumin does not differentiate the posterior cingulate areas particularly well, except for the retrosplenial areas as noted below. In this regard, area 23d and both divisions of area 23 have two plexi in layers III and V that do not vary substantially in this region.

Posterior cingulate and retrosplenial cortices

Although the posterior cingulate gyrus has been considered above, the composition of areas 23c, f 23c, 31, and 7m have not been addressed nor have the dorsal and ventral divisions of PCC been considered in detail. Area 23c on the dorsal bank of the cingulate gyrus (Fig.11; 1) has a broad external granular layer in relation to the deeper layers, dense layers II and IV, extensive NFP-expressing layer IIIc pyramids, and a poorly differentiated layer V; all of which distinguish it from area 24d rostrally. The fundal division of area 23c is similar to its dorsal bank counterpart, although the lamination is greatly attenuated.

Areas 23a/b are not uniform in the dorsoventral plane or "z" axis. The dorsal areas d23a/b are relatively thinner than their ventral counterparts and have a slightly more-dense layer Va. As shown in Figure 9 (NeuN), area v23b has much thicker layers IIIc, IV, and V, and it has many more NFP-ir neurons (SMI32) in layers IIIc and Va, and they are substantially larger than is the case for area d23b. The NeuN and SMI32 images were merged by reducing the opacity of the SMI32 image and magnifying both by 1.5× to show the exact position of the SMI32-ir neurons in both areas. Although all pairs of NeuN and SMI32 images were so coregistered to ensure exact coregistration of images, the present ones are provided for these areas to show the accurate coregistration in the presence of an intervening layer IV. This method emphasizes that the density of NFP-ir neurons is very substantially higher in layer IIIc of v23b and layers IIIc-V are thicker than is the case for areas d23a or d23b.

Area 31 surrounds the spls and has the most extensive layers II, IIIab, and IV of any cingulate area. Comparison of areas 31 and 7m in Figure 11 shows much greater NFP-ir in layer IIIc of area 7m, a dense layer IV, and a thinner layer Vb. Higher magnification of layers IIIc–Va shows that neurons throughout mid-cortical layers of area 7m appear to be stacked. The example of one such formation at the arrow was 37 neurons in length from layer IV to its apex in layer IIIc, and its total length was 375 μm. Of course, neurons form similar aggregates in all cingulate areas; however, those in area 7m are much longer and contribute in a meaningful way to the low-magnification cytoarchitecture.

Architecture of the retrosplenial areas 29 and 30 has been documented thoroughly in both human and monkey; however, a few comments in the present context including parvalbumin expression need consideration. The highest level of NFP expression in retrosplenial cortex is in layer VI and to a lesser extent in layer V of area 29l as shown in Figure 12. The granular neurons of layer III/IV in both areas 29l and 29m do not express these proteins. Because the laminar position of SMI32 immunoreactivity can be difficult to assess, the images were merged with NeuN as shown in Figure 12 to show the exact position of labeled neurons. The only NFP immunoreactivity in superficial layers of area 29 is associated with labeled dendrites from deep lying pyramidal neurons. Area 29l has extremely rich parvalbumin expression, making this marker ideal for locating the border between 29l and 29m. Indeed, the labeling of somata and processes is so dense that laminar differentiation is not possible in the former. Finally, area 30 is dysgranular as shown in human (Vogt et al., 2001). The variability of layer IV, interdigitation of layer IIIc neurons with those in layer Va, and heavy expression of NFPs by large layer IIIc pyramids is the same as in human. Interestingly, parvalbumin expression is almost entirely located in layers II–III with a predominance in layer II. This pattern of labeling is not present in any anterior or midcingulate area.

Horizontal plane of section

Horizontal sections show similar architectures at high magnifications; however, borders between areas on the gyral surface can be identified in macrophotographs of single sections and confirm observations of different architectures in separate coronal sections. Figure 13 shows a macrophotograph through the dorsal part of the cingulate gyrus with progressive differentiation from rostral area 24b to caudal area 31. Layer Va in the NeuN sample (Fig. 13A) is emphasized with arrows to show the progression from thin and relatively sparse in area 24b (1) to a thicker and more neuron-dense composition particularly in areas p24b′, 23d, and d23b (3, 4). Progressive changes in the expression of neurofilament proteins are also shown Figure 13B, where arrows are used to emphasize changes in layer IIIc. Before arrow 5 in Figure 13, the SMI32 immunoreactive neurons are sparse in layer IIIc and tend to be solitary. The border of areas p24b′ and 23d is heralded by heavy expression of NFP by layer IIIc pyramidal neurons starting at arrow 5. The sixth arrow emphasizes

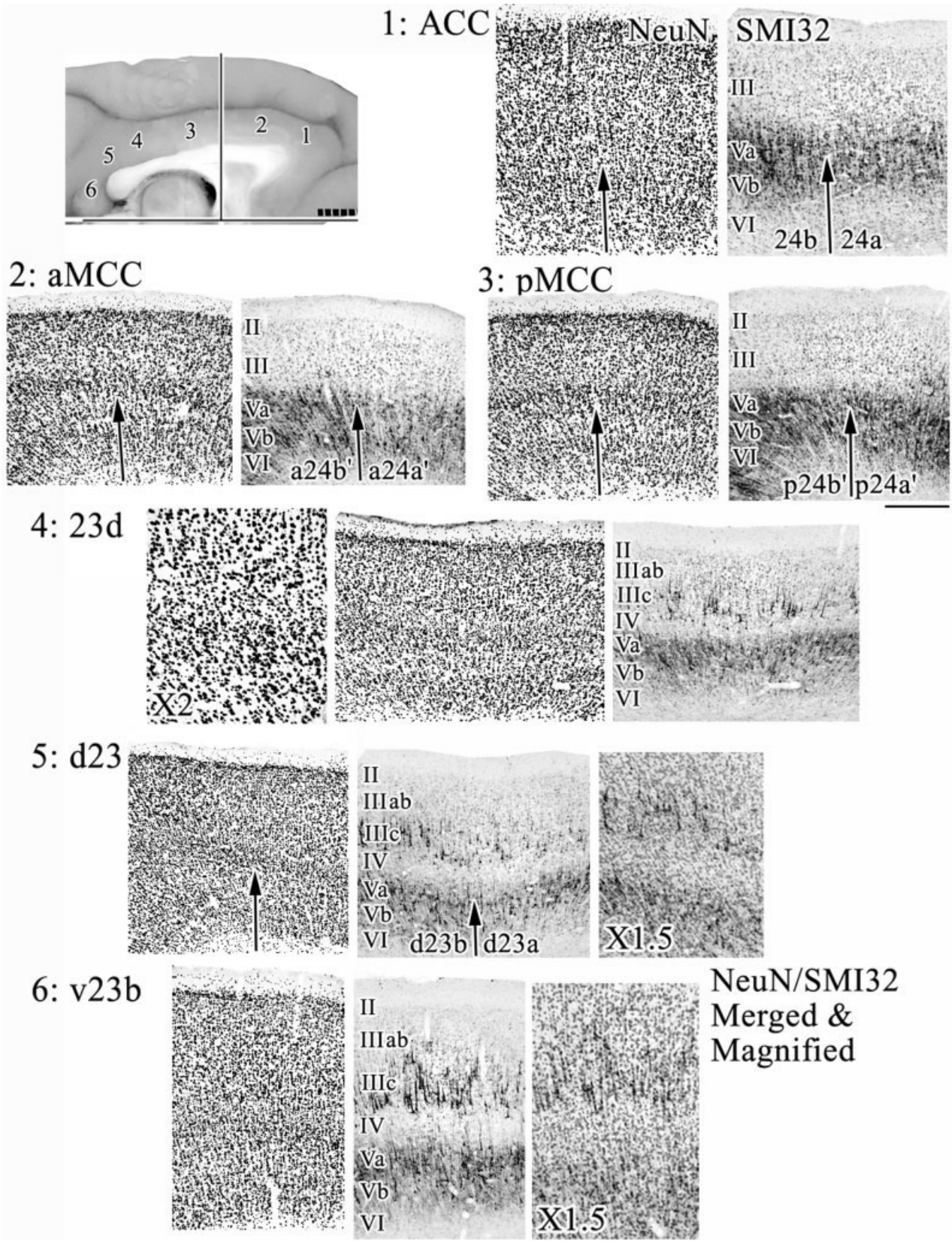

Fig. 9. Architecture and cytology of cortex along the surface of the cingulate gyrus. Comparisons of the "a" and "b" divisions are enhanced with the vertical arrows to the border of layers IIIc and Va. Dysgranular area 23d has a variable layer IV and relatively even distribution of NFP-immunoreactive neurons in layers IIIc and Va. Layer IV is magnified (2×) to show the dysgranular nature of this cortex with the interdigitation of layer IIIc and Va pyramids. Differences between the dorsal and ventral parts of area 23 are shown with levels 5 and 6. To ensure exact coregistration of the layers, the opacity of the SMI32 photographs was reduced and the NeuN image merged with it at increased magnification (1.5×). For abbreviations, see list. Scale bar = 500 μm.

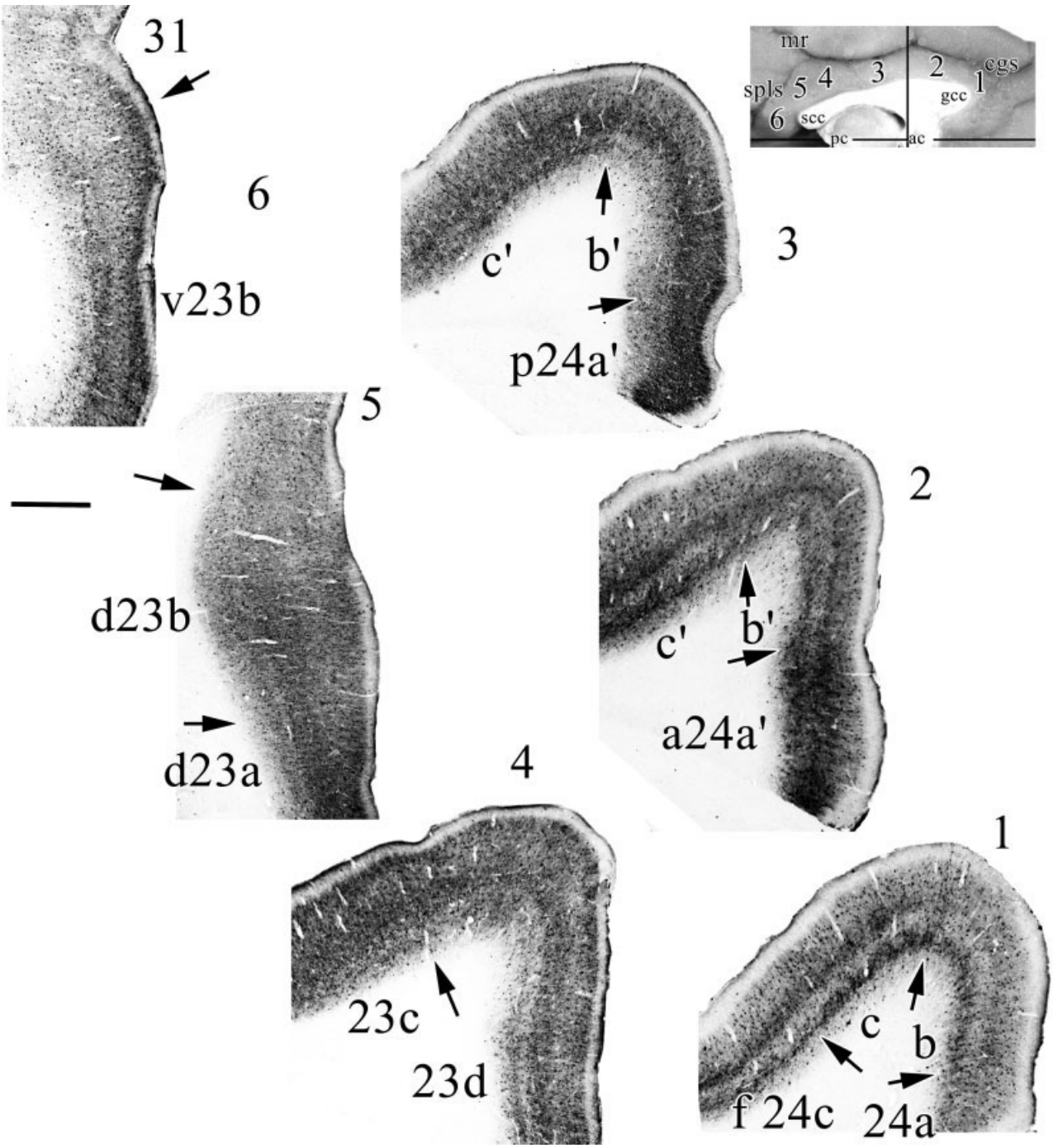

Fig. 10. Parvalbumin-immunoreactivity is helpful for identifying areas in anterior and midcingulate cortices, whereas it is less valuable with areas 23 and 31. For example, level 1 shows the four divisions of area 24 at the genu of the corpus callosum. Even differences between a24′ and p24′ can be seen with the broader layer Va and more diffuse plexi in the latter areas. For abbreviations, see list. Scale bar = 1 mm.

the intermingling of NFP-expressing neurons in layer IIIc with those in layer Va in dysgranular area 23d. Area d23b has a more-dense expression of neurons in both layers IIIc and Va, whereas those in both layers of area 31 are among the highest in the cingulate gyrus. Each of these laminar observations can be verified above with high magnification and in the coronal plane of section.

DISCUSSION

The present analysis of monkey cingulate gyrus architecture and neurocytology builds upon a rich base of human anatomical and functional studies, and it appears that the fundamental organization of monkey cingulate cortex is similar to that in human. Particular new findings

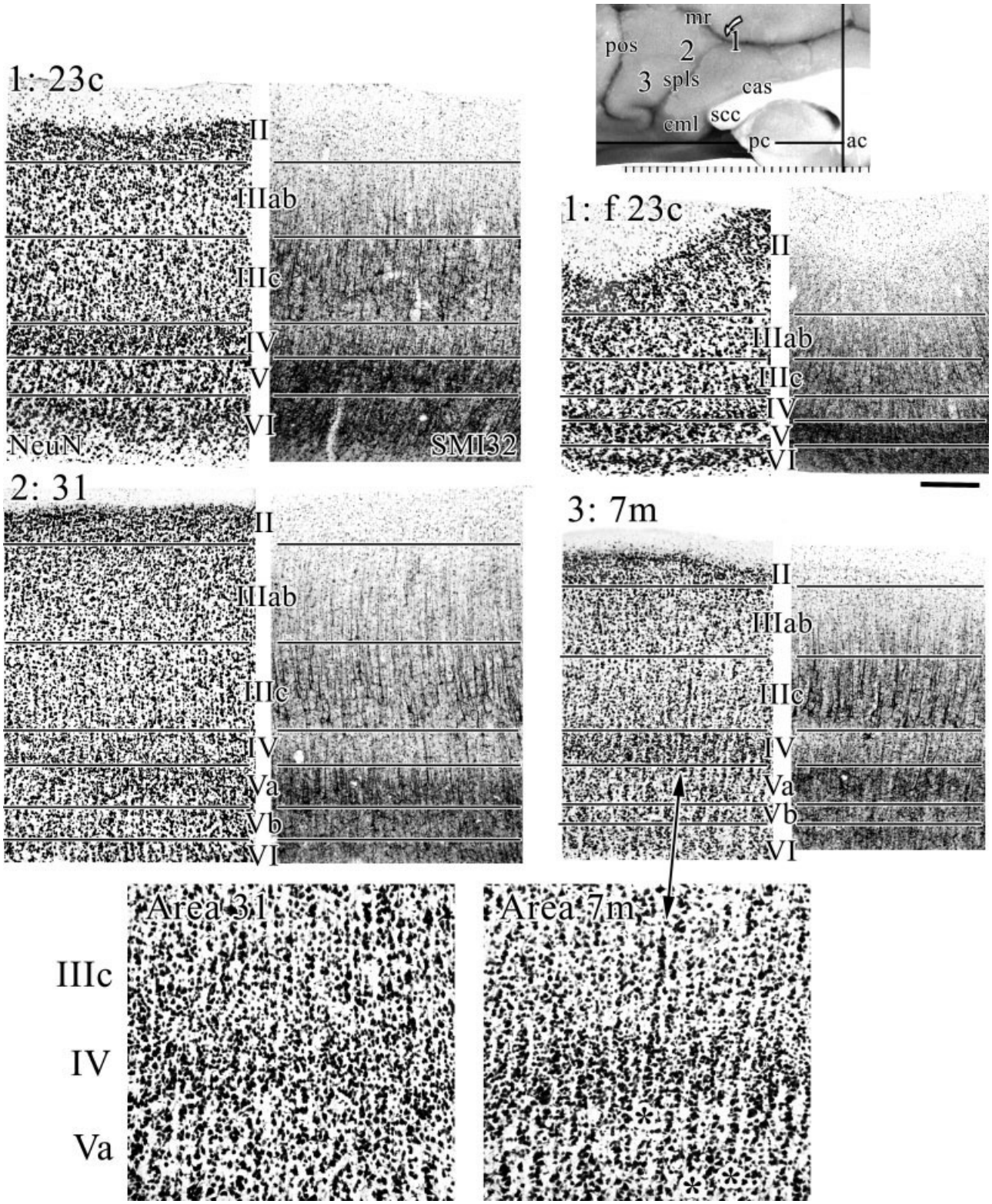

Fig. 11. Dorsal parts of PCC (1) at area 23c, 2 at area 31, and 3 at medial parietal area 7m. Area 23c has a disproportionately broad superficial layer and compressed layer V. Area 31 has the thickest layer IV of any cingulate area and high densities of layer IIIc NFP-expressing neurons. Area 7m has a much broader layer IV than area 31, very large and dense, NFP-expressing, layer IIIc pyramids, and small neurons that extend into layer IIIc. The stacking of neurons in mid-cortical layers is characteristic of area 7m (asterisks; magnification 2×) and not of area 31. For abbreviations, see list. Scale bar = 250 μm.

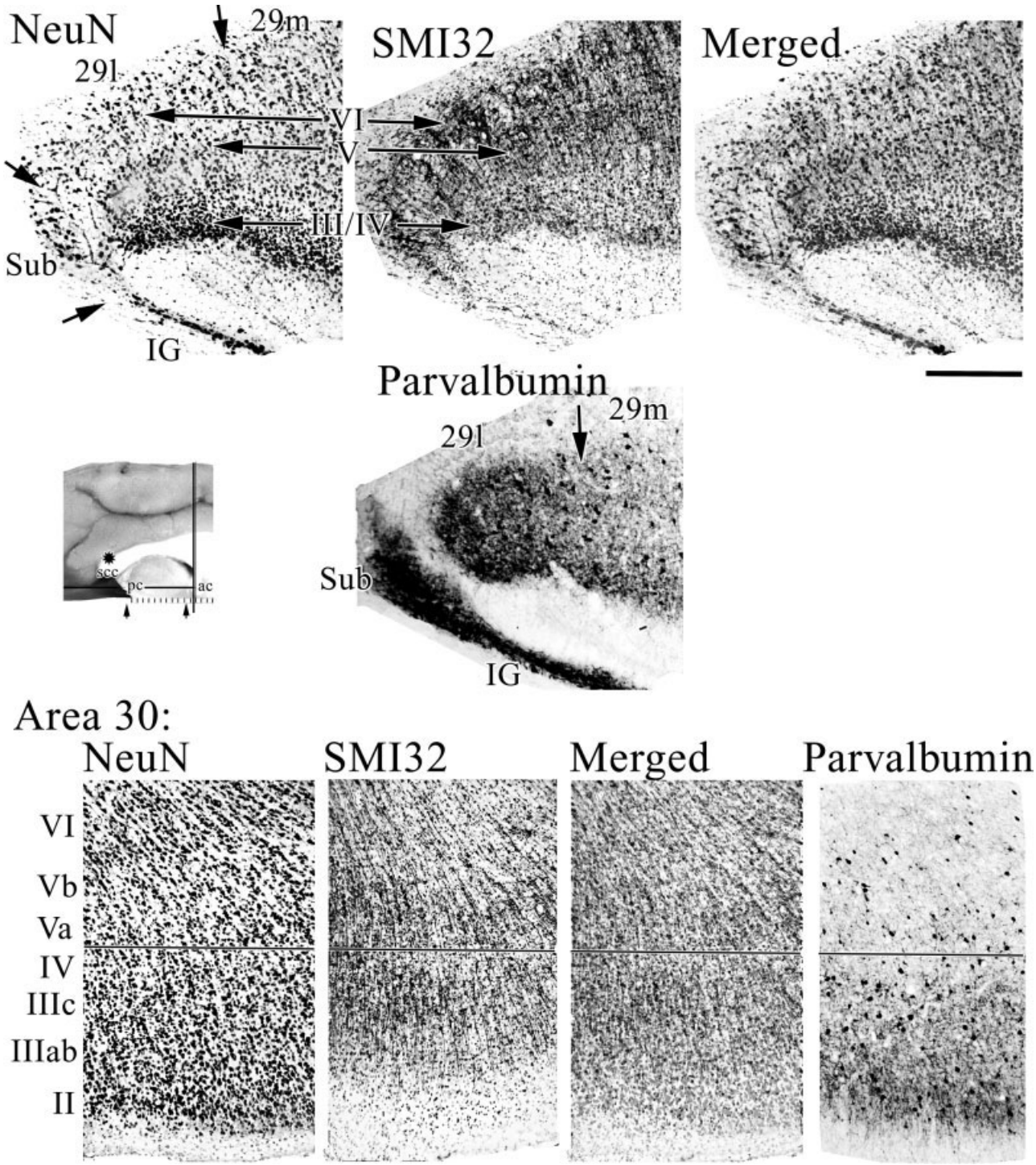

Fig. 12. Retrosplenial areas are well defined with NeuN, SMI32, and parvalbumin. Indeed, the massive intrinsic parvalbumin system is very robust in area 29l. Neurons in the granular layer (i.e., layer III/IV) do not express NFP, and this is documented by merging images from NeuN and SMI32. Area 30 is dysgranular as seen with NeuN, and the highest level of NFP expression is in layers IIIc and Va as emphasized in the merged sections. For abbreviations, see list. Scale bar = 500 μm.

in monkey include (1) two divisions of MCC (a24′ and p24′); (2) two divisions of PCC (d23 and v23); (3) fundal extensions of all areas on the dorsal bank of the cingulate gyrus, however, no cingulate areas are formed on the dorsal bank of the cingulate sulcus; (4) parvalbumin is a useful marker of areas in ACC and RSC, although less useful for divisions of PCC; and (5) area 23d is a dysgranular transition area between areas p24a′/b′ and d23a/b.

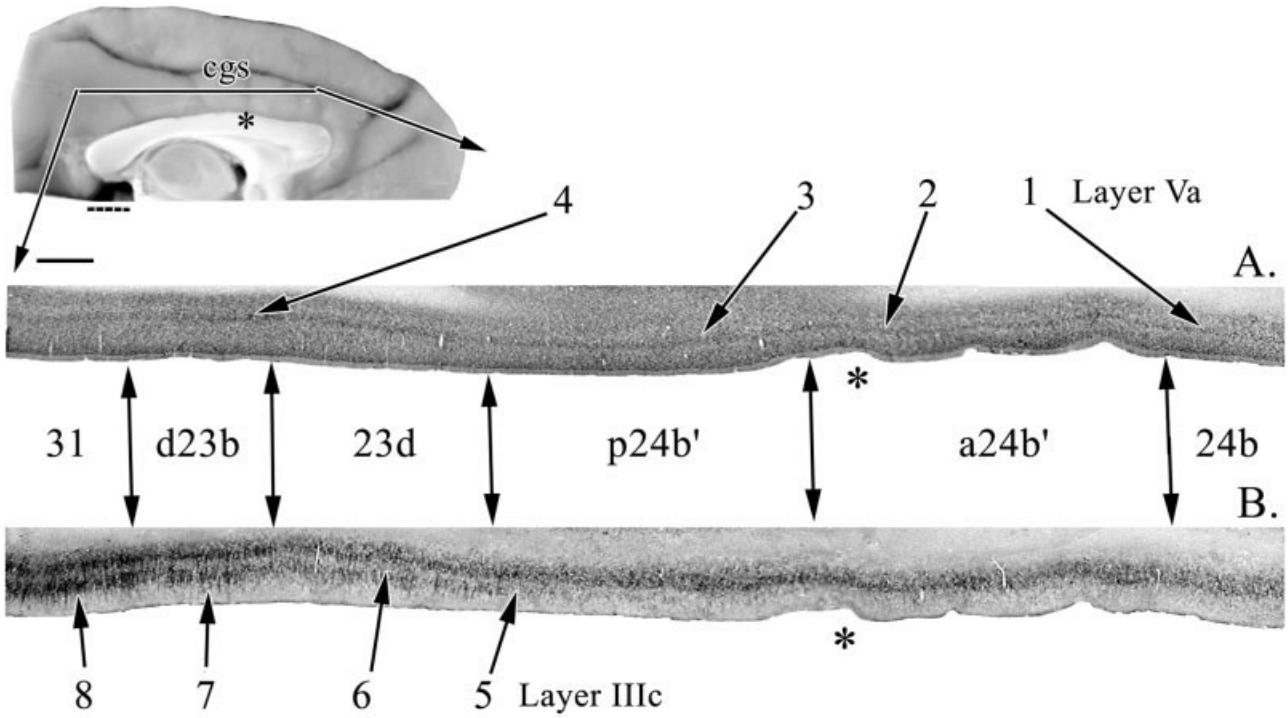

Fig. 13. The dorsal part of the cingulate gyrus shows progressive differentiation from area 24b to area 31. The asterisk on the medial surface orients to the same dimple in each section. **A:** Layer Va in NeuN is emphasized with arrows to show progression from thin and relatively sparse (1) to a thicker and more neuron-dense composition (3, 4). **B:** Progressive changes in the expression of NFP is shown, where arrows emphasize changes in layer IIIc from sparse SMI32+ neurons in layer IIIc to the border of areas p24b′ and 23d with heavy expression of NFP by layer IIIc pyramidal neurons (5). Area d23b has a more-dense expression of neurons in both layers IIIc and Va, whereas those in both layers of area 31 are among the highest density and intensity in the cingulate gyrus (8). For abbreviations, see list. Scale bar = 1 mm/division (above), 1 mm (below).

Flat maps of area distributions on the cingulate gyrus can be used for direct comparisons of connection and motor system organization.

Anterior cingulate region

The four-region model of the cingulate gyrus places ACC in a perigenual position in human (Vogt et al., 2004) and monkey (Vogt et al., 1997), and this and other changes have been introduced in the ACC since the original map was published in 1987. First, area 24a in the monkey appears to be the major area caudal to area 32 with little or no contribution of area 24b as suggested by Carmichael and Price (1994). These latter investigators also demonstrated a medial extension of area 10 termed area 10m ventral to area 32, and this finding was confirmed in the present study with all three markers. Braak (1979) evaluated the perigenual region in human pigment architecture preparations and referred to it as a magnocellular area. Review of the structure of area 24a in this region in monkey suggests that it does not have disproportionately large neurons. Rather, the largest neurons lie in each fundal division of the dorsal bank of the cingulate gyrus, including those in area f 24c.

The role of ACC in autonomic regulation is well-known and serves as an important criterion for defining this region as separate from MCC (Neafsey et al., 1993; Vogt et al., 1997). The subgenual part of ACC is activated during sad events in healthy human subjects (Mayberg, 1997; Phan et al., 2002; Vogt et al., 2003), and in major depression, this region has altered neuronal activity and may explain mood-congruent processing disruption with reduced responses to happiness when compared with controls and elevated responses during sadness (Elliott et al., 2002). Of interest, sadness activity occurred ventral to the genu in healthy individuals, whereas happiness was more rostral (Vogt et al., 2003).

It is important that another key rationale for the ACC/MCC dissociation is the selective vulnerability of ACC to major depression. Glucose metabolism is reduced in this region in major depression (Drevets, 2001); however, differences in glucose metabolism for drug responders and nonresponders occurs dorsal in it (Mayberg et al., 1997). At present, the entire ACC must be viewed as vulnerable to depression, whereas MCC appears to have no such vulnerability. Although there is conflicting evidence for a structural basis for depression (Harrison, 2002), the organization, connections, and chemistry of this region in monkey and its potential to develop a model of depression makes further assessment of ACC pivotal to understanding human neuronal diseases.

Midcingulate cortex

The most profound change to the concept of monkey cingulate cortex deriving from the present work is that MCC is a unique division. Although first proposed as a transitional region in monkey (Vogt, 1993), this view needs to be extended as in human. Area 24′ is more than

a structural transition cortex, because it represents a unique structural region with specific functions that differentiate it from the other regions. Moreover, it composes fully one third of the entire cingulate gyrus. Thus, area 24′ represents more than a simple transitional region; it is a unique region, and the MCC conveys this intention rather than the view of a transition area. Two points about cingulate regionalization of structure and function flow from this perspective. First, transition between ACC and PCC is not due to a simple deposition of more neurons in layer IV as suggested by Brodmann (1909), Vogt et al. (1987), and Morecraft et al. (2004). According to further comments below, there is a progression that actually starts with differentiation of layer Va before addition of a dysgranular area 23 and the granular areas 23 and 31. Second, the concept of MCC emphasizes its unique role as a skeletomotor control region with specific architectures, projection neurons, and functional responses, including nociceptive ones.

In view of the ACC/MCC differentiation in the monkey, it is possible to use the monkey to model particular neuronal diseases. The MCC in human is selectively vulnerable to chronic neuropathic and lower-back pain syndromes (Hsieh et al., 1995; Derbyshire et al., 1994, 2002), whereas syndromes associated with psychiatric symptoms selectively impact ACC as discussed above. Thus, this differential vulnerability to neuronal disease is a key criterion for differentiating ACC and MCC, and their presence in monkey is yet another tool for studying human disease processes.

Cingulate motor areas

Braak (1976) first demonstrated a CMA with his primitive gigantopyramidal field. A similar area in monkey was identified and termed area 24d (Matelli et al., 1991); it was shown to have large and NFP-ir neurons in layer Vb (Nimchinsky et al., 1996), and it has a topographically organized motor field (Rizollatti et al., 1996). The organization of sulcal cortex, however, is quite complex, and the anatomical composition and functions of this region are still a matter of active research and debate. Zilles et al. (1996) observed that the caudal cingulate motor area in human (cCMA; area 24d) is composed of two divisions; cmc1 and cmc2. Area cmc1 is caudal to the latter and has much larger neurons in layers III and V. The present monkey observations are in agreement with those of Zilles et al. (1995; 1996) in the human. Thus, area cmc1 equates to area 24d and cmc2 to area p24c′.

To evaluate the projections and electrically stimulated movements in the context of the current observations, Figure 14 shows the flat map coregistered to findings of Rizzolatti et al. (1996) and Dum and Strick (1991). Although the overlap is only approximate, several interesting suggestions emerge from comparing these various reports. Rizzolatti et al. (1996) extended area 24d rostrally to include much of our area p24c′. Much of area 24d is involved in forelimb, upper trunk, and neck movement, whereas area p24c′ appears to be involved in hindlimb, lower trunk, and tail movements. Notice that Matelli et al. (1991) included a rostral extension of our fp24c′ in their area 24d. Of interest, area fp24c′ has the largest neurons in the cingulate gyrus. We fully agree with the localization of area 23c by Matelli et al. (1991) and notice that it had no evoked activity (Rizzolatti et al. (1996). Therefore, area 23c may not contain a CMA as suggested by Morecraft et al. (2004), although it may have some corticospinal projection neurons.

Figure 14 provides a comparison of current findings with those of Dum and Strick (1991). Although the coregistration is approximate, it appears that corticospinal projections originate from area 23c, even though stimulation-evoked movements were not observed by Rizzolatti et al. (1996). The greatest density of corticospinal projection neurons is in areas p24c′ and fp24c′; the latter of which we observed to have the largest, layer-Vb, pyramidal neurons. Finally, corticospinal projections are prominent from area a24c′ and very limited from area 24c. The two cingulate motor areas likely reside in areas 24d/p24c′ (cCMA) and area a24c′ (rCMA).

It has been proposed that there is a third CMA on the dorsal bank of the caudal cingulate sulcus termed area 6c or "dCMA" (Dum and Strick, 1993; He et al., 1995). No cortex dorsal to the fundal divisions has a "cingulate" motif (e.g., large and dense layer Va relative to layer IIIc in NeuN, and heavier NFP immunoreactivity in layer Va than layer IIIc). It appears that cortex on the dorsal bank of the cgs is composed of ventral divisions of areas 6aβ and 6aα (or area 6c according to Dum and Strick and He et al.) rather than cingulate cortex as observed in human brain (Vogt and Vogt, 2003). Therefore, this dorsal cortex is either part of the supplementary motor system or it is a unique extension thereof. Russo et al. (2002) attempted to evaluate the "dCMA" and suggested similarities between it and the cCMA. Although no medial surface landmarks are provided, it appears that 13 of their 18 presumptive "dCMA" units were in the fundal part of area p24c′ rather than on the dorsal bank of the cgs per se; only two units were on the dorsal bank. Thus, there is not yet adequate evidence for a third CMA in the dorsal bank of the caudal cingulate sulcus, and it will likely not be a "cingulate" motor area if it is found. This conclusion raises further issues, however, particularly in terms of whether or not there is a single somatotopic map that extends across the dorsal and ventral banks of the cgs. Labeling of cortical projection neurons and electrical stimulation suggests a single map in the cCMA that may extend beyond cingulate cortex (Wang et al., 2001). This explanation suggests that cortical and intrinsic processing must be substantially different for regions involving forelimb and upper trunk versus hindlimb and lower trunk projection cortex. The extremely dense NFP-expressing neurons in layer IIIc of areas 6c/v6aβ suggest a very different phenotype for each bank of the cgs.

Although the organization of cingulate motor cortex is becoming quite clear, it does appear that each area has substantial intrinsic variability. What is the interpretation of widely variable cytoarchitectures in a single, somatotopically organized motor field? Although it is true that corticospinal projections provide a unifying feature of the cingulate motor areas (Dum and Strick, 1991, 1993), structural differences within a motor field suggest they have different intrinsic organization and contribute to additional functions. In other words, cortex of the cCMA may contribute to cognitive functions beyond simple skeletomotor regulation. The present findings suggest that the monkey cCMA does not have an extension onto the dorsal bank of the cingulate sulcus as in human (Vogt et al., 2004) and that cortex subsuming the cCMA includes areas 24d and p24c′, which may equate to cmc1 and cmc2,

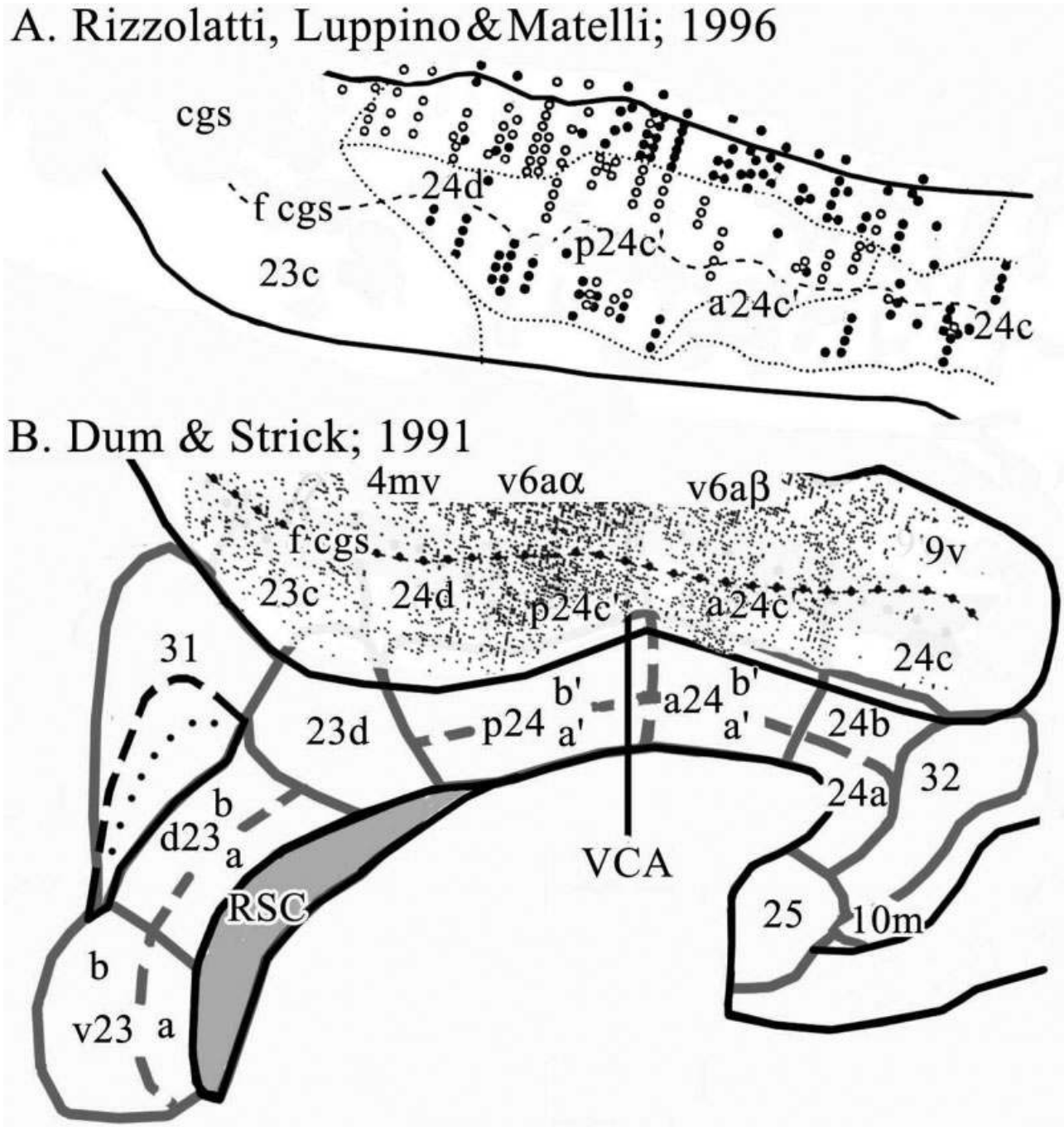

Fig. 14. The flat map coregistered to the findings of other investigators. A,B: In view of the pivotal nature of corticospinal projections in the cingulate sulcus, electrical stimulation (A, modified from Rizzolatti et al., 1996) and labeling of corticospinal projection neurons (B, modified from Dum and Strick, 1991) were coregistered to the flat map. In both cases, the dashed line represents the fundus of the cingulate sulcus. **A:** The open circles represent sites that activated hindlimb–lower trunk–tail movements, whereas the filled circles evoked forelimb–upper trunk–neck movements. Nonresponsive sites are not shown for ease of comparison. **B:** The density of labeled neurons is shown after a horseradish peroxidase injection into the cervical spinal cord to produce a relatively complete labeling of corticospinal projection neurons. In both instances, area designations are shown to correlate with matches and mismatches between our findings and previous observations in the cingulate sulcus. For abbreviations, see list.

respectively, of Zilles et al. (1996). There also are the two fundal extensions of each of these areas, which always contain larger neurons in layers IIIc and Vb than do their ventral bank counterparts. Anatomical variations in the cingulate motor fields may lead to a new view of cognitive–motor interactions (Murtha et al., 1996; Bush et al., 2002).

Because the fundal extensions of the CMAs have profoundly distorted architectures due to cortical curvature, it is unlikely that they contribute equally to function like other parts of the motor fields. Indeed, in addition to having the largest pyramidal neurons in the cingulate gyrus, the density and size of parvalbumin-expressing neurons is substantially greater in fundal divisions. Because fundal areas 24d and p24c′ participate in skeletomotor regulation, it might be posited that cingulate motor function is based on the organization of the fundal regions and that additional architectures encountered on the dorsal bank of the cingulate gyrus represent additional circuitry for cognitive processing. The substantial variation in structural organization even within a single cingulate motor area predicts new functions for these areas, which extend beyond simple motor output.

Dysgranular cortex and cingulate transitions

Area 30 is a dysgranular transitional cortex between areas 29m and 23a that has heavy and reciprocal connections with area 23a (Vogt and Pandya, 1987). Because the present study also demonstrated a dysgranular area 23d between areas p24a′/b′ and d23a/b that is continuous with area 30 of RSC, there appears to be a dysgranular transition zone between the agranular and periallocortical regions of the cingulate gyrus. One of the most important issues raised in the past decade of human cytological research is the location of the border between anterior agranular area 24 and posterior granular area 23. The Brodmann map shows a rather simple and sharp transition from an agranular area 24 to a granular area 23, and this is reflected in our earlier map (Vogt et al., 1987); a thorough re-analysis of this case does not show such a simple transition. In the context of pMCC, the transition between these two fundamentally different types of cortex can be detailed: (1) Between areas a24′ and p24′ layer Va has a substantial increase in the number of small neurons in layer Va. (2) Between areas p24′ and 23d, there is an additional dysgranular layer IV. (3) Between areas 23d and 23a/b, there is an increase in the breadth of layer IV. Of interest, even in granular area 23 in NeuN preparations, layer Va is more prominent than is layer IV, because of the granularity of the former. (4) Between areas d23a/b and 31, there is a profound increase in the breadth of layer IV and a shift in larger pyramids to layer IIIc from layer Va. In addition to this latter change, the density of NFP-expressing neurons in layer IIIc also increases substantially. Thus, the Brodmann map misidentifies the point of transition from agranular area 24 to granular area23, and the complex features of transition between anterior and posterior cingulate cortices have been thoroughly defined for both monkey and human brains.

Dorsal and ventral PCC

Circuitry and functional studies show differentiation of PCC into two parts, yet no cytoarchitectural studies have analyzed whether or not there is a structural substrate for it. Thus, auditory inputs arrive to dPCC from caudal area TA and those to vPCC from rostral area TA (Yukie, 1995). Prefrontal cortex projections from the dorsal bank of the principal sulcus terminate in dPCC, whereas cortex in the rostral tip of both banks projects to vPCC (Vogt and Barbas, 1988). Shibata and Yukie (2003) reported that each PCC division has unique thalamic connections with the dPCC receiving inputs from the central laterocellular, mediodorsal, and ventral anterior and ventral lateral nuclei that do not project to the vPCC. Finally, neurocytology in the human cortex using techniques similar to those of the present study also showed a cytological and functional difference between these areas (Vogt et al., personal communication).

The morphological substrate for defining the two parts of area 23 include the many more and larger neurons in layers IIIc and V, more NFP-expressing neurons in these layers, and the much thicker layer IV in area v23 than in d23. These are the same features that distinguish these areas in human (Vogt et al., personal communication). The vPCC region has direct and reciprocal interactions with subgenual ACC (Vogt and Pandya, 1987), and this linkage provides for direct interchanges of information between these two regions. Because the former is involved in affect and emotion, as discussed in the introduction, and the latter is involved in visuospatial orientation, it is possible that information interchanges by means of the vPCC are associated with the personal relevance of previously coded sensory events.

LITERATURE CITED

Akkal D, Audin J, Burbaud P. 2002. Comparison of neuronal activity in the rostral supplementary and cingulate motor areas during a task with cognitive and motor demands. Eur J Neurosci 15:887–904.

Baleydier C, Mauguiere F. 1980. The duality of the cingulate gyrus in monkey: neuroanatomical study and functional hypothesis. Brain 103: 525–554.

Biber MP, Kneisley LW, LaVail JH. 1978. Cortical neurons projecting to the cervical and lumbar enlargements of the spinal cord in young and adult rhesus monkeys. Exp Neurol 59:492–508.

Braak H. 1976. A primitive gigantopyramidal field buried in the depth of the cingulate sulcus of the human brain. Brain Res 109:219–233.

Braak H. 1979. Pigment architecture of the human telencephalic cortex. V. Regio anterogenualis. Cell Tissue Res 204:441–451.

Broca P. 1878. Anatomie comparée circonvolutions cérébrales: Le grande lobe limbique et la scissure limbique dans la série des mammifères. Rev Anthropol Ser 21:384–498.

Brodmann K. 1909. Vergleichende Lokalisationslehre der Grosshirnrinde in ihren Prinzipien dargestellt auf Grund des Zellenbaues. Leipzig: Barth.

Bush G, Vogt BA, Holmes J, Dale AM, Greve D, Jenike MA, Rosen BR. 2002. Dorsal anterior cingulate cortex: a role in reward-based decision-making. Proc Natl Acad Sci U S A 99:523–528.

Carmichael ST, Price JL. 1994. Architectonic subdivision of the orbital and medial prefrontal cortex in the macaque monkey. J Comp Neurol 346:366–402.

Derbyshire SWG, Jones AKP, Devani P, Friston KJ, Feinman C, Harris M, Watson JD, Frakowiak RSJ. 1994. Cerebral responses to pain in patients with atypical facial pain measured by positron emission tomography. J Neurol Neurosurg Psychiatry 57:1166–1172.

Derbyshire SWG, Jones AKP, Creed F, Starz T, Meltzer CC, Townsend DW, Peterson AM, Firestone L. 2002. Cerebral responses to noxious thermal stimulation in chronic low back pain patients and normal controls. Neuroimage 16:158–168.

Dombrowski SM, Hilgetag CC, Barbas H. 2001. Quantitative architecture distinguishes prefrontal cortical systems in the rhesus monkey. Cereb Cortex 11:975–988.

Drevets WC. 2001. Neuroimaging and neuropathological studies of depression: implications for the cognitive-emotional features of mood disorders. Curr Opin Neurobiol 11:240–249.

Dum RP, Strick PL. 1991. The origin of corticospinal projections from the premotor areas in the frontal lobe. J Neurosci 11:667–689.

Dum RP, Strick PL. 1993. Cingulate motor areas. In: Vogt BA, Gabriel M, editors. Neurobiology of cingulate cortex and limbic thalamus. Boston: Birkhauser. p 415–441.

Elliott R, Rubinsztein JS, Sahakian BJ, Dolan RJ. 2002. The neural basis

of mood-congruent processing biases in depression. Arch Gen Psychiatry 59:597–604.

Harrison PJ. 2002. The neuropathology of primary mood disorder. Brain 125:1428–1449.

He S-Q, Dum RP, Strick PL. 1995. Topographic organization of corticospinal projections from the frontal lobe: motor areas on the medial surface of the hemisphere. J Neurosci 15:3284–3306.

Hsieh J-C, Belfrage M, Stone-Elander S, Hansson P, Ingvar M. 1995. Central representation of chronic on going neuropathic pain studied with positron emission tomography. Pain 63:225–236.

Luppino G, Matelli M, Camarda RM, Gallese V, Rizzolatti G. 1991. Multiple representations of body movements in mesial area 6 and the adjacent cingulate cortex: An intracortical microstimulation study in the macaque monkey. J Comp Neurol 311:463–482.

MacLean PD. 1990. The triune brain in evolution, role in paleocerebral functions. New York: Plenum Press.

Matelli M, Luppino G, Rizzolatti G. 1991. Architecture of superior and mesial Area 6 and the adjacent cingulate cortex in the macaque monkey. J Comp Neurol 311:445–462.

Mayberg HS. 1997. Limbic-cortical dysregulation: a proposed model of depression. J Neuropsychiatry 9:471–480.

Mayberg HS, Brannan SK, Mahurin RK, Jerabek PA, Tekell JL, McGinnis S, Glass TG, Martin CC, Fox PT. 1997. Cingulate function in depression: a potential predictor of treatment response. Neuroreport 8:1057–1061.

Morecraft RJ, Van Hoesen GW. 1992. Cingulate input to the primary and supplementary motor cortices in the rhesus monkey: evidence for somatotopy in Areas 24c and 23c. J Comp Neurol 322:471–489.

Morecraft RJ, Cipollomi PB, Stilwell-Morecraft KS, Gedney MT, Pandya DN. 2004. Cytoarchitecture and cortical connections of the posterior cingulate and adjacent somatosensory fields in the rhesus monkey. J Comp Neurol 469:37–69.

Murtha S, Chertkow H, Beauregard M, Dixon R, Evans A. 1996. Anticipation causes increased blood flow to the anterior cingulate cortex. Hum Brain Map 4:103–112.

Neafsy EJ, Terreberry RR, Hurley KM, Ruit KG, Frysztak RJ. 1993. Anterior cingulate cortex in rodents: connections, visceral control functions, and implications for emotion. In: Vogt BA, Gabriel M, editors. Neurobiology of cingulate cortex and limbic thalamus. Boston: Birkhauser. p 206–223.

Nimchinsky EA, Hof PR, Young WG, Morrison JH. 1996. Neurochemical, morphologic, and laminar characterization of cortical projection neurons in the cingulate motor areas of the macaque monkey. J Comp Neurol 374:136–160.

Nimchinsky EA, Vogt BA, Morrison JH, Hof PR. 1997. Neurofilament and calcium-binding proteins in the human cingulate cortices. J Comp Neurol 384:597–620.

Papez JW. 1937. A proposed mechanism of emotion. Arch Neurol Psychiatry 38:725–733.

Phan KL, Wager T, Taylor SF, Liberzon I. 2002. Functional neuroanatomy of emotion: a meta-analysis of emotion activation in PET and fMRI. Neuroimage 16:331–348.

Rizzolatti G, Luppino G, Matelli M. 1996. The classic supplementary motor area ids formed by two independent areas. Adv Neurol 70:45–56.

Rose M. 1927. Gyrus limbicus anterior and Regio retrosplenialis (Cortex holoprotoptychos quinquestratificatus) Vergleichende Architektonik bei Tier und mensch. J Psycol Neurol 43:65–173.

Russo GS, Backus DA, Ye S, Crutcher MD. 2002. Neural activity in monkey dorsal and ventral cingulate motor areas: Comparison with the supplementary motor area. J Neurophysiol 88:2612–2629.

Shibata H, Yukie M. 2003. Differential thalamic connections of the posteroventral and dorsal posterior cingulate gyrus in the monkey. Eur J Neurosci 18:1615–1626.

Shima K, Tanji J. 1998. Role for cingulate motor area cells in voluntary movement selection based on reward. Science 282:1335–1338.

Shima K, Aya K, Mushiake H, Inase M, Aizawa H, Tanji J. 1991. Two movement-related foci in the primate cingulate cortex observed in signal-triggered and self-paced forelimb movements. J Neurophysiol 65:188–202.

Smith GE. 1907. A new topographical survey of the human cerebral cortex, being an account of the distribution of the anatomically distinct cortical areas and their relationship to the cerebral sulci. J Anat 41:237–254.

Takada M, Tokuno H, Hamada I, Inase M, Ito Y, Imanishi M, Hasegawa N, Akazawa T, Hatanka N, Nambu A. 2001. Organization of inputs from cingulate motor areas to basal ganglia in macaque monkey. Eur J Neurosci 14:1633–1650.

Van Hoesen GW, Morecraft RJ, Vogt BA. 1993. Connections of the monkey cingulate cortex. In: Vogt BA, Gabriel M, editors. Neurobiology of cingulate cortex and limbic thalamus. Boston: Birkhauser. p 249–284.

Vogt BA. 1993. Structural organization of cingulate cortex: areas, neurons, and somatodendritic transmitter receptors. In: Vogt BA, Gabriel M, editors. Neurobiology of cingulate cortex and limbic. Boston: Birkhauser. p 19–70.

Vogt B, Barbas H. 1988. Structure and connections of the cingulate vocalization region in the rhesus monkey. In: Newman JD, editor. The physiological control of mammalian vocalization. New York: Plenum Press. p 203–225.

Vogt BA, Pandya DN. 1987. Cingulate cortex of the rhesus monkey: II. Cortical afferents. J Comp Neurol 262:271–289.

Vogt BA, Vogt L. 2003. Cytology of human dorsal midcingulate and supplementary motor cortices. J Chem Neuroanat 26:301–309.

Vogt BA, Rosene DL, Pandya DN. 1987. Cingulate cortex of the rhesus monkey: I. Cytoarchitecture and thalamic afferents. J Comp Neurol 262;256–270.

Vogt BA, Finch DM, Olson CR. 1992. Functional heterogeneity of cingulate cortex: The anterior executive and posterior evaluative regions. Cereb Cortex 2:435–443.

Vogt BA, Nimchinsky EA, Vogt LJ, Hof PR. 1995. Human cingulate cortex: surface features, flat maps, and cytoarchitecture. J Comp Neurol 359: 490–506.

Vogt BA, Vogt LJ, Nimchinsky EA, Hof PR. 1997. Primate cingulate cortex chemoarchitecture and its disruption in Alzheimer's disease. In: Bloom FE, Bjorklund A, Hokfelt T, editors. Handbook of chemical neuroanatomy, the primate nervous system. Vol. 13. Part I. Amsterdam: Elsevier. p 455–528.

Vogt BA, Berger GR, Derbyshire SWG. 2003. Structural and functional dichotomy of human midcingulate cortex. Eur J Neurosci 18:3134–3144.

Vogt BA, Hof PR, Vogt L. 2004. Cingulate gyrus. In: Paxinos G, Mai J, editors. The human nervous system. 2nd ed. San Diego: Elsevier. p 915–945.

Vogt BA, Vogt LJ, Perl DP, Hof PR. 2001. Cytology of human caudomedial cingulate, retrosplenial, and caudal parahippocampal cortices. J Comp Neurol 438:353–376.

Vogt C, Vogt O. 1919. Allgemeinere Ergebnisse unserer Hirnforschung. J Psychol Neurol 25:279–461.

von Economo C, Koskinas GN. 1925. Die Cytoarchitectonik der Hirnrinde des erwachsenen Menschen. Berlin: Springer.

Vorobiev V, Govoni P, Rizzolatti G, Matelli M, Luppino G. 1997. Parcellation of human mesial area 6: cytoarchitectonic evidence for three separate areas. Eur J Neurosci 10:2199–2203.

Wang Y, Shima K, Sawamura H, Tanji J. 2001. Spatial distribution of cingulate cells projecting to the primary supplementary and presupplementary motor areas: a retrograde multiple labeling study in the macaque monkey. Neurosci Res 39:39–49.

Yukie M. 1995. Neural connections of auditory association cortex with the posterior cingulate cortex in the monkey. Neurosci Res 22:179–187.

Zilles K, Schlaug G, Matelli M, Luppino G, Schleicher A, Qu M, Dabringhaus A, Seitz R, Roland PE. 1995. Mapping of human and macaque sensorimotor areas by integrating architectonic, transmitter receptor, MRI and PET data. J Anat 187:515–537.

Zilles K, Schlaug G, Geyer S, Luppino G, Matelli M, Qü M, Schleicher A, Schormann T. 1996. Anatomy and transmitter receptors of the supplementary motor areas in the human and nonhuman primate brain. Adv Neurol 70:29–43.